

A Model Predictive Capture Point Control Framework for Robust Humanoid Balancing via Ankle, Hip, and Stepping Strategies

Myeong-Ju Kim¹, Daegy Lim¹, Gyeongjae Park¹, and Jaeheung Park^{1,2}

Abstract—The robust balancing capability of humanoid robots against disturbances has been considered as one of the crucial requirements for their practical mobility in real-world environments. In particular, many studies have been devoted to the efficient implementation of the three balance strategies, inspired by human balance strategies involving ankle, hip, and stepping strategies, to endow humanoid robots with human-level balancing capability. In this paper, a robust balance control framework for humanoid robots is proposed. Firstly, a novel Model Predictive Control (MPC) framework is proposed for Capture Point (CP) tracking control, enabling the integration of ankle, hip, and stepping strategies within a single framework. Additionally, a variable weighting method is introduced that adjusts the weighting parameters of the Centroidal Angular Momentum (CAM) damping control over the time horizon of MPC to improve the balancing performance. Secondly, a hierarchical structure of the MPC and a stepping controller was proposed, allowing for the step time optimization. The robust balancing performance of the proposed method is validated through extensive simulations and real robot experiments. Furthermore, a superior balancing performance is demonstrated, particularly in the presence of disturbances, compared to a state-of-the-art Quadratic Programming (QP)-based CP controller that employs the ankle, hip, and stepping strategies. The supplementary video is available at <https://youtu.be/CrD75UBYzdc>

Index Terms—Humanoid walking control, push recovery, capture point (CP) control, model predictive control (MPC), and three balance strategies (ankle, hip, and stepping strategies).

I. INTRODUCTION

HUMANOID robots have been studied to achieve human-like walking capability in environments designed for human activities. However, their ability to adapt to disturbances caused by uneven terrain and potential collisions remains a challenge. To navigate these environments successfully, a robust balance control strategy that overcomes disturbances and ensures safe locomotion is essential.

In order to attain robust balancing performance in humanoid robots, researchers have been inspired by human balance strategies, and several researches are conducted to study them [1]–[3]. The imitation and analysis of human balance strategies, including ankle, hip, and stepping strategies, have been

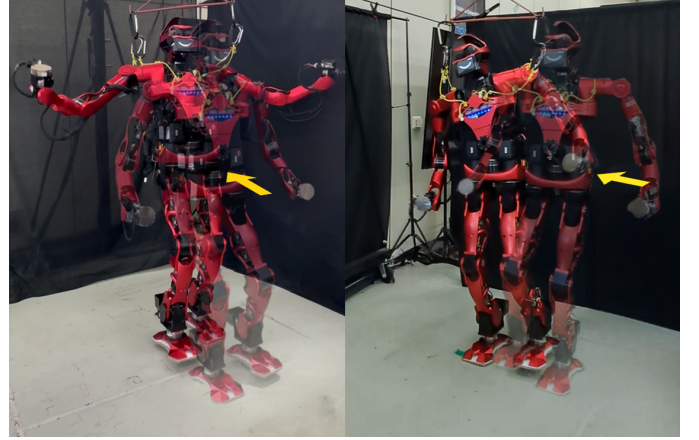


Fig. 1: Dynamic balancing of humanoid robot using ankle, hip, and stepping strategies in the presence of disturbances.

explored using a simple model [4]–[6]. The lessons learned from these investigations have been applied to humanoid robot research, with each strategy being implemented in a distinct manner. Specifically, the ankle strategy has been implemented through the Zero Moment Point (ZMP) control and the hip strategy has been implemented using Centroidal Angular Momentum (CAM) control. Lastly, the stepping strategy has been realized through the stepping control, which adjusts footstep position or step time.

In the early days of humanoid walking research, many studies were conducted to control ZMP, which is frequently referred to as an ankle strategy, by utilizing a simplified model. The Linear Inverted Pendulum Model (LIPM) [7], [8] was introduced, which simplifies the dynamics of complex humanoid robots, and the linear relationship between the Center of Mass (CoM) and ZMP [9], [10] is established. Many studies aimed to minimize the error between the reference ZMP and the actual ZMP, premised on the concept that if the ZMP is positioned within the support region, the robot will remain stable [11]–[15]. Kajita et al. [11] proposed a preview control method that considers a future reference ZMP trajectory, which compensates for ZMP errors by generating CoM trajectories. Choi et al. [12] calculates the desired CoM velocity to regulate ZMP and CoM errors, and utilizes the CoM Jacobian to generate the desired CoM velocity. Kim et al. [13] proposed a state observer-based ZMP feedback controller that accounts for the joint elasticity of the robot. Kajita et

This work was supported by the National Research Foundation of Korea (NRF) grant funded by the Korea government (MSIT) (No. 2021R1A2C3005914).

¹Myeong-Ju Kim, Daegy Lim, Gyeongjae Park and Jaeheung Park are with the Department of Intelligence and Information, Seoul National University, Republic of Korea. Contact : park73@snu.ac.kr

²Jaeheung Park is also with the Advanced Institutes of Convergence Technology, Republic of Korea and with ASRI, RICS, Seoul National University, Republic of Korea.

al. [14] calculates contact wrenches to track the reference ZMP and utilized an admittance control method to generate the calculated contact wrenches. Joe et al. [15] proposed a comprehensive ZMP control framework that combines the state feedback controller suggested in [13] with the contact wrench controller proposed in [14]. While these studies have greatly contributed to the research on balancing in humanoid walking, the robot's ability to maintain balance relies only on ZMP control whose balancing capacity is limited by the size of the supporting polygon. Therefore, additional strategies were necessary to withstand strong disturbances.

Studies have been conducted to enhance the balancing capabilities of humanoid robots by exploring not only the ankle strategy utilizing ZMP control but also the hip strategy utilizing the robot's upper body. The hip strategy is commonly used in humanoids to control the CAM with the upper body. To account for the angular momentum that was disregarded in the LIPM, simple models such as Angular Momentum inducing inverted Pendulum Model (AMPM) or Linear Inverted Pendulum Plus Flywheel Model (LIPFM) have been proposed [16]–[18], and the dynamic relationship between the CoM and Centroidal Moment Pivot (CMP) has been defined [18]. Based on this, many CAM control frameworks have been proposed to overcome external disturbances [19]–[24]. Yi et al. [20] proposed a CAM control framework that generates a desired CAM through the hip joint and sequentially recovers the initial pose at a predetermined time when the CoM is perturbed by external disturbances. Schuller et al. [22] proposed a CAM control framework based on whole-body dynamics, in which the CAM tracking control and initial pose return control are operated by soft hierarchy-based Quadratic Programming (QP) optimization. In our previous CAM control approach [23], we addressed the issue of degraded balancing performance caused by the conflict between initial pose control and CAM tracking control arising from the soft hierarchy in [22] by utilizing a control framework based on Hierarchical Quadratic Programming (HQP). Ding et al. [24] proposed a CAM controller that plans arm trajectories to improve balancing performance using the Model Predictive Control (MPC) approach. These methods have been shown to improve balancing performance. However, the amount of CAM generation in a robot is constrained by the joint limit of the robot and the self-collision avoidance, which in turn affects the robot's ability to maintain balance.

The stepping control, which adjusts the footstep position or step time in an adaptive manner to disturbances, has greatly improved the balancing performance of humanoid robots compared to the conventional walking control based on pre-determined footsteps and step time [25]–[31]. Under the notion that the position of the CoM converges to the Capture Point (CP) using LIPM dynamics, several stepping algorithms have been proposed [26], [27], [29], [30]. Khadiv et al. [26], [30] proposed a framework that employs QP optimization based on the CP end-of-step dynamics to calculate the footstep position and step time. This approach tracks the pre-planned CP offset during walking by adjusting the footstep position and step time. Jeong et al. [27], [29] proposed a stepping control method that also utilizes CP end-of-step dynamics, where the ankle torque is pre-calculated in response to external

disturbances, and the step time and footstep position are optimized accordingly. Furthermore, many control frameworks have been proposed for adjusting footstep position against disturbances by utilizing MPC optimization [25], [28], [31]. Herdt et al. [25] proposed an MPC framework that extends the framework proposed by Wieber et al. [32], by automatically adjusting the footstep position to control the CoM velocity and the ZMP error. Joe et al. [28] proposed a framework for adjusting footstep position when the desired ZMP generated to reduce ZMP error is limited by ZMP constraints. The continuous evolution of stepping algorithms has significantly contributed to humanoid balance control.

With the advancement of each balance control strategy, many studies have been proposed with the aim of integrating these strategies to enhance balancing capability [33]–[36]. Shafiee-Ashtiani et al. [33] proposed a linear MPC framework that builds upon the MPC-based stepping controller suggested by [25] to combine three balance strategies (ankle, hip, and stepping strategies). In this approach, the ZMP and CoM velocity control problem proposed in [25] was changed to a ZMP and CP control problem. Furthermore, the control inputs were expanded to include change of the centroidal moment, resulting in improved control performance. Ding et al. [34], [35] proposed a nonlinear MPC framework using a nonlinear Inverted Pendulum Flywheel (IPF) model. By considering the nonlinear relationship between CoM and ZMP in IPF as a quadratic constraint, the method adjusts the ZMP and body angles, as well as the footstep position to compensate for large disturbances. Romualdi et al. [36] proposed a nonlinear MPC framework for disturbance rejection based on centroidal dynamics, which involves the control of contact wrench, CAM, and footstep position. These studies developed a robust walking framework to cope with disturbances by integrating the three balance strategies through MPC. However, they did not consider step time adjustment algorithms, which play a crucial role in withstanding disturbances.

Studies that included the three balance strategies and a step time adjustment were also proposed [37]–[39]. Aftab et al. proposed an MPC-based balance control framework that integrates three balance strategies and step time adjustment to address disturbances [37]. To avoid a biased output of the smallest step time during step time optimization, a swing foot acceleration cost was introduced to adjust the step time appropriately. However, due to the nonlinearity arising from step time optimization, the algorithm could not be used in real-time and was only applicable to standing situations, not in the walking control. Nazemi et al. proposed a reactive walking pattern generator based on hierarchical structure [38]. In this approach, the stepping controller proposed by [26], [30] is first used to determine the footstep position and step time for the stepping strategy. Subsequently, the CP trajectory and body angle were adjusted using MPC to track the reference ZMP trajectory determined by the pre-planned footstep position and step time. Jeong et al. [39] proposed a QP-based optimization method to achieve three balance strategies with step time adjustment for controlling the CP end-of-step. In this method, to avoid the variable coupling during the linearization for QP, the ZMP control input for ankle strategy was pre-

computed using the instantaneous CP control method [40], rather than through optimization. Based on this pre-computed ZMP control input, the CAM control and stepping control are performed through QP optimization. In [38], [39], the robust balancing performance was validated against disturbances through simulations or experiments. However, three balance strategies cannot be computed from a single framework in [38], [39]. Additionally, these methods are unable to consider future states and constraints beyond the current walking step, which can affect the balancing performance. This limitation arises from the control framework relying on CP end-of-step dynamics, which restricts the prediction horizon to the current step duration.

In this paper, a robust balance control framework is proposed to overcome disturbances through the integration of three balance strategies and step time optimization (as shown in Fig. 1). In contrast to [38], [39], our research does not restrict the horizon time of MPC based on the current step duration. The proposed framework expands upon our prior works [23], [31] that were developed for the same goal, i.e., CP tracking control. We combined the hip strategy in [23] and the ankle and stepping strategies in [31] into a single MPC framework. With novel ideas, we addressed several technical problems that arose during the integration process, thereby enhancing the coherence between control hierarchies in the proposed control framework. The primary contributions of this paper can be summarized as follows:

- 1) An MPC framework that integrates three balance strategies for CP tracking control is proposed. The proposed MPC framework is an extension of the MPC framework proposed in our prior work [31]. Unlike [31], the proposed framework includes MPC optimization to handle not only ZMP control and stepping control but also CAM control. Furthermore, this framework enables more effective CAM control through MPC, unlike the heuristic CAM calculation method based on CMP decomposition proposed in our previous study [23]. To the best of our knowledge, the proposed MPC is the first integrated MPC framework for CP tracking control that implements all three balance strategies. Our approach differs from [33] in that in our MPC framework, footstep position control is driven by CP control instead of ZMP control.
- 2) A novel variable weighting method for CAM control is proposed. This method adjusts the weighting parameters of CAM damping control during the time horizon of the MPC to enhance the CP control performance and demonstrates better balancing performance compared to the conventional constant weighting method.
- 3) A hierarchical structure of the proposed MPC and stepping controller enables optimization of step time. Furthermore, an approach for determining stepping control parameters based on the MPC is suggested, which achieves better control performance than the previous parameter selection approach [26], [30], [31].
- 4) The proposed method is validated through extensive simulations and real robot experiments using our humanoid

robot, TOCABI. Additionally, when compared to a state-of-the-art QP-based CP controller that incorporates three balance strategies [39], the proposed method demonstrates superior balancing performance in the presence of disturbances.

This paper is organized as follows. In Section II, we briefly introduce the LIPFM and CP dynamics that underlie the walking control framework proposed in this paper. In Section III, an overview of the walking control framework is introduced. Section IV provides a detailed description of the MPC framework proposed in this paper, while Section IV-C introduces the variable weighting method proposed in this paper. Section V describes the proposed MPC-based stepping controller. In Section VI, the results of simulations and real robot experiments conducted to validate and analyze the proposed algorithm are presented. Finally, in Section VII, the conclusion of this paper is presented. Subsequently, we shall refer to the proposed MPC framework as CP-MPC for the remainder of this paper.

II. FUNDAMENTALS

A. Linear Inverted Pendulum Plus Flywheel Model

The LIPFM is a linear abstract model that was developed to address the CAM of humanoid robots [18]. The LIPFM assumes that the total mass of the robot is concentrated at the CoM, and the height of the CoM from the ground is considered to be constant. Unlike the LIPM [7], [8], the LIPFM is capable of handling reaction torque by means of the rotational motion of a flywheel located at the CoM. The dynamic equation of the LIPFM is expressed in terms of the relationship between the CoM and the CMP, and is defined as follows,

$$\ddot{c}_x = \omega^2(c_x - p_x), \quad (1)$$

$$p_x = z_x + \frac{\tau_y}{mg}, \quad (2)$$

where c_x , p_x , and z_x denote the positions of CoM, CMP, and ZMP in the x -direction, respectively. $\omega = \sqrt{g/c_z}$ is the natural frequency, g is the gravitational acceleration, and c_z is the height of the CoM from the ground. τ_y represents the reaction torque of the flywheel in the y -direction. A detailed derivation of LIPFM dynamics is presented in [18].

The dynamics of LIPFM in the y -direction can also be derived in the same way as the x -direction, and the dynamics in each direction can be dealt with independently. This decoupling property of the system simplifies the analysis and control of the system and makes it easier to handle each direction separately. Therefore, in this study, the dynamics were derived only in the x -direction for conciseness of the paper, except for Section V, where the step time variable couples both x - and y -direction variables.

B. Capture Point dynamics based on LIPFM

This section provides a brief introduction to the CP dynamics based on LIPFM. The concept of CP, introduced in [18], [41], has been extensively utilized in various studies as a control variable for stabilizing the CoM of a robot and as

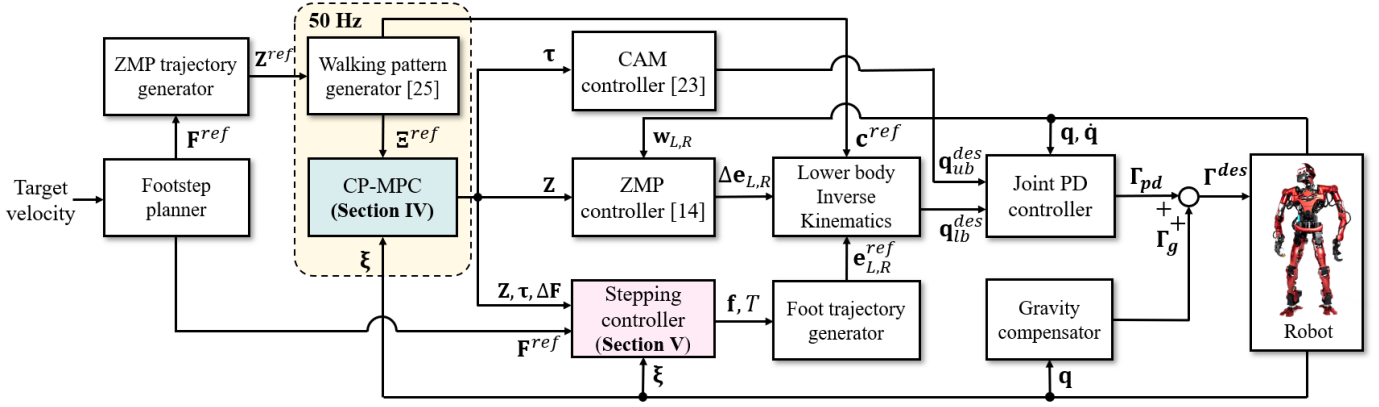


Fig. 2: Overall control framework for robust humanoid walking; Three balance strategies are employed for CP tracking control based on the CP-MPC, and next footstep position and step time are determined by the stepping controller.

an indicator of its balance state [15], [21], [27], [28], [40], [42]–[44]. The dynamics of the CP is expressed as a linear combination of horizontal position and velocity of the CoM as below,

$$\dot{\xi}_x = c_x + \frac{\dot{c}_x}{\omega}, \quad (3)$$

where ξ_x represents the CP in the x-direction. The LIPFM also allows the CP to be expressed as a dynamic relationship with the CMP. By combining (1) with the time derivative of (3), the dynamics of the CP-CMP can be derived as

$$\dot{\xi}_x = \omega(\xi_x - p_x) = \omega(\xi_x - (z_x + \frac{\tau_y}{mg})). \quad (4)$$

Assuming a constant value of the CMP, p_x , within a walking step duration of T , and considering the time elapsed after the start of the swing phase as t , the behavior of the CP can be defined as follows,

$$\xi_{x,T} = (\xi_x - p_x)e^{\omega(T-t)} + p_x. \quad (5)$$

Equation (5), known as the CP end-of-step dynamics [29], [39], [40], provides a means to predict the CP at the end of a current step by using the current CP, current time, and CMP as inputs.

In Section IV, the CP-CMP dynamics (4) is employed as a prediction model in the proposed CP-MPC. Additionally, the CP end-of-step dynamics (5) is utilized for the stepping controller presented in Section V.

III. OVERALL WALKING CONTROL STRUCTURE

This section provides the overview of the proposed walking control framework. The schematic diagram of the overall walking control framework is illustrated in Fig. 2. First, the footstep planner determines the positions of footstep, $\mathbf{F}^{ref} = [\mathbf{F}_x^{ref} \ \mathbf{F}_y^{ref}]$, based on the target velocity command. Using the footstep positions as input, the ZMP trajectory generator generates reference ZMP trajectories, $\mathbf{Z}^{ref} = [\mathbf{Z}_x^{ref} \ \mathbf{Z}_y^{ref}] \in \mathbb{R}^{N \times 2}$. The walking pattern generator then takes these reference ZMP trajectories as input and produces reference CP trajectories, $\Xi^{ref} = [\Xi_x^{ref} \ \Xi_y^{ref}] \in \mathbb{R}^{N \times 2}$.

The main goal of CP-MPC is to track the reference CP trajectories. The CP-MPC receives the reference CP trajectories

as its control target and generates three optimized MPC variables, including ZMP control inputs, $\mathbf{Z} = [\mathbf{z}_x \ \mathbf{z}_y] \in \mathbb{R}^{N \times 2}$, centroidal moment control inputs, $\boldsymbol{\tau} = [\boldsymbol{\tau}_y \ -\boldsymbol{\tau}_x] \in \mathbb{R}^{N \times 2}$, and footstep adjustments, $\Delta \mathbf{F} = [\Delta \mathbf{F}_x \ \Delta \mathbf{F}_y] \in \mathbb{R}^{m \times 2}$, from \mathbf{F}^{ref} to track these trajectories. Note that N represents the prediction horizon for the CP-MPC, while m denotes the number of pre-designed footsteps within the prediction horizon, N .

The ZMP controller [14] computes desired contact wrenches to achieve the desired ZMP, $\mathbf{z}^{des} = [z_x^{des} \ z_y^{des}] \in \mathbb{R}^2$, which is the first element of the ZMP control inputs, \mathbf{Z} . Subsequently, the admittance controller compares the measured contact wrench, $\mathbf{w}_{L,R} \in \mathbb{R}^6$, with the desired contact wrench to determine the changes of the position and orientation of the support foot with respect to the pelvis, $\Delta \mathbf{e}_{L,R} \in \mathbb{R}^6$. The subscript L and R signify the left and right, respectively.

The stepping controller calculates the next footstep position, $\mathbf{f} = [f_x \ f_y] \in \mathbb{R}^2$, and the step time, T , to achieve the footstep adjustment, $\Delta \mathbf{f}_1 = [\Delta f_{x,1} \ \Delta f_{y,1}] \in \mathbb{R}^2$, planned by CP-MPC. Specifically, the controller primarily adjusts the step time, T , based on CP end-of-step dynamics (5) to ensure that the \mathbf{f} achieves $\Delta \mathbf{f}_1$ as closely as possible. Here, $\Delta \mathbf{f}_1$ refers to the first element of $\Delta \mathbf{F}$, representing the adjustment of the next footstep. The detailed explanation is described in Section V. After determining \mathbf{f} and T , the foot trajectory generator creates reference foot trajectories, $\mathbf{e}_{L,R}^{ref} \in \mathbb{R}^6$. Consequently, the lower body inverse kinematics is solved for the desired joint angles of legs, \mathbf{q}_{lb}^{des} , required to achieve the reference CoM trajectories, $\mathbf{c}^{ref} \in \mathbb{R}^3$, reference foot trajectories, $\mathbf{e}_{L,R}^{ref} \in \mathbb{R}^6$, and displacement of the support foot pose, $\Delta \mathbf{e}_{L,R} \in \mathbb{R}^6$. In addition, when a step change occurs, the footstep planner generates footsteps based on the target velocity command relative to the supporting foot.

The desired centroidal moment, $\boldsymbol{\tau}^{des} = [\boldsymbol{\tau}_y^{des} \ -\boldsymbol{\tau}_x^{des}] \in \mathbb{R}^2$, which is the first element of the centroidal moment control inputs, $\boldsymbol{\tau}$, is controlled by the HQP-based CAM controller proposed in our previous study [23]. The desired centroidal moment, $\boldsymbol{\tau}^{des}$, is integrated to yield the desired CAM, and the HQP-CAM controller computes the desired upper body joint angles, \mathbf{q}_{ub}^{des} , to achieve the desired CAM.

In the final stage, the joint PD controller is employed to calculate the joint torques required to track the upper and lower body motions. These computed joint torques, Γ_{pd} , are then commanded to the joints in conjunction with the gravity compensation torque, Γ_g .

IV. CP-MPC: MODEL PREDICTIVE CONTROL FRAMEWORK FOR CAPTURE POINT TRACKING

In our previous study [31], we proposed a linear MPC framework that controls the ZMP and footstep position to follow the CP trajectory (ankle and stepping strategies). In [31], the CP control performance, which was previously limited by the ZMP constraint in the MPC of [45], was improved by relaxing the ZMP constraint through the adjustment of footstep position.

In this work, we extend the framework of our previous study [31] to propose CP-MPC, the MPC framework that incorporates three balance strategies: ankle, hip, and stepping strategies. The proposed CP-MPC utilizes not only the ZMP and footstep position but also the centroidal moment to enhance the CP control performance against strong external disturbances. Detailed explanations of the proposed MPC framework are provided in the following subsections.

A. Prediction of Future Trajectory

In order to formulate the CP-MPC, the CP-CMP dynamics described in (4) is utilized as a prediction model. Equation (4) can be discretized with the piecewise ZMP, centroidal moment, and sampling time T_s as below,

$$\xi_{x,k+1} = A\xi_{x,k} + \mathbf{B} [z_{x,k} \quad \tau_{y,k}]^T \quad (6)$$

where $A = e^{\omega T_s}$, $\mathbf{B} = \begin{bmatrix} 1 - e^{\omega T_s} & \frac{1 - e^{\omega T_s}}{mg} \end{bmatrix}$. The CMP, p_x , can be decomposed into ZMP, z_x , and centroidal moment, τ_y , as shown in (4), and two variables are independently treated as control inputs of the CP-MPC.

By recursive application of (6), the predicted future trajectories of CP over the time horizon, N , that emanate from the current CP, $\xi_{x,k}$, can be expressed as below,

$$\Xi_x = \Phi_\xi \xi_{x,k} + \Phi_p \mathbf{P}_x, \quad (7)$$

$$\Phi_\xi = \begin{bmatrix} A \\ \vdots \\ A^N \end{bmatrix}, \quad \Phi_p = \begin{bmatrix} A^0 B & \cdots & 0 \\ \vdots & \ddots & \vdots \\ A^{N-1} B & \cdots & A^0 B \end{bmatrix}, \quad (8)$$

$$\Xi_x = \begin{bmatrix} \xi_{x,k+1} \\ \vdots \\ \xi_{x,k+N} \end{bmatrix}, \quad \mathbf{P}_x = \begin{bmatrix} z_{x,k} \\ \tau_{y,k} \\ \vdots \\ z_{x,k+N-1} \\ \tau_{y,k+N-1} \end{bmatrix}. \quad (9)$$

$\Xi_x \in \mathbb{R}^N$ represents the predicted future CP trajectory in the x-direction and $\mathbf{P}_x \in \mathbb{R}^{2N}$ denotes the future inputs of the ZMP and centroidal moment. The matrix $\Phi_\xi \in \mathbb{R}^N$ defines the dynamic relationship between the current CP, $\xi_{x,k}$, and future CP trajectory, Ξ_x . The matrix $\Phi_p \in \mathbb{R}^{N \times 2N}$

defines the relationship between future inputs, \mathbf{P}_x , and future CP trajectory, Ξ_x . In \mathbf{P}_x , to handle each control input independently, we represent the series of ZMP vectors as $\mathbf{Z}_x = [z_{x,k} \ z_{x,k+1} \ \cdots \ z_{x,k+N-1}]^T \in \mathbb{R}^N$, and the series of centroidal moment vectors is represented as $\boldsymbol{\tau}_y = [\tau_{y,k} \ \tau_{y,k+1} \ \cdots \ \tau_{y,k+N-1}]^T \in \mathbb{R}^N$.

B. Problem Setup for MPC Optimization

This section presents the problem formulation for MPC optimization. The cost function and constraints of the proposed CP-MPC framework are formulated as follows,

$$\min_{\mathbf{P}_x, \Delta \mathbf{F}_x} \quad \|\Xi_x - \Xi_x^{ref}\|_{\mathbf{w}_\xi}^2 + \|\boldsymbol{\tau}_y + \mathbf{K}_d \mathbf{h}_y\|_{\mathbf{w}_\tau}^2 \quad (10)$$

$$\begin{aligned} & + \|\Delta \mathbf{F}_x\|_{\mathbf{w}_F}^2 + \|\Delta \mathbf{P}_x\|_{\mathbf{w}_p}^2 \\ \text{s. t.} \quad & \underline{\mathbf{Z}}_x \leq \mathbf{A}_p \begin{bmatrix} \mathbf{Z}_x \\ \Delta \mathbf{F}_x \end{bmatrix} \leq \bar{\mathbf{Z}}_x \\ & \underline{\boldsymbol{\tau}}_y \leq \boldsymbol{\tau}_y \leq \bar{\boldsymbol{\tau}}_y \\ & \Delta \underline{\mathbf{F}}_x \leq \Delta \mathbf{F}_x \leq \Delta \bar{\mathbf{F}}_x \end{aligned} \quad (11)$$

with

$$\mathbf{A}_p = [\mathbf{I}_N \quad -\mathbf{S}], \quad \mathbf{S} = \begin{bmatrix} s_{1,1} & s_{1,2} & \cdots & s_{1,m} \\ \vdots & \vdots & \ddots & \vdots \\ s_{N,1} & s_{N,2} & \cdots & s_{N,m} \end{bmatrix}.$$

The cost function in (10) is composed of four cost terms in total. The first cost term functions as a reference CP trajectory tracking control and is weighted by a positive diagonal weighting matrix, $\mathbf{w}_\xi \in \mathbb{R}^{N \times N}$. The second cost term generates the damping centroidal moment that drives the desired CAM to zero when the magnitude of the disturbance is small. Here, $\mathbf{K}_d \in \mathbb{R}^{N \times N}$ is a damping matrix which is positive and diagonal and $\mathbf{h}_y \in \mathbb{R}^N$ is the CAM in y-direction which is an integration of $\boldsymbol{\tau}_y$. This term is weighted by a positive diagonal matrix, $\mathbf{w}_\tau \in \mathbb{R}^{N \times N}$. The diagonal terms of \mathbf{w}_τ are adjusted based on the magnitude of the ZMP control inputs to improve the CP control performance. This adjustment algorithm is explained in Section IV-C. The third cost term regulates the additional footsteps adjustment from the pre-planned footsteps. This term is weighted by a positive diagonal matrix, $\mathbf{w}_F \in \mathbb{R}^{m \times m}$. The last cost term regulates the change of the control input to prevent rapid changes and generate a smooth control input. This term is weighted by positive diagonal matrix, $\mathbf{w}_p \in \mathbb{R}^{2N \times 2N}$. The MPC variables consist of \mathbf{P}_x and $\Delta \mathbf{F}_x$, where $\mathbf{P}_x \in \mathbb{R}^{2N}$ represents the ZMP and centroidal moment input sequence, and $\Delta \mathbf{F}_x = [\Delta f_{x,1} \ \Delta f_{x,2} \ \cdots \ \Delta f_{x,m}]^T \in \mathbb{R}^m$ represents a vector consisting of additional footstep adjustments in the x-direction.

The constraints in (11) consist of three inequality conditions. The first constraint refers to the ZMP constraint, which confines the ZMP control input, $\mathbf{Z}_x \in \mathbb{R}^N$, within the support polygon. The vectors $\bar{\mathbf{Z}}_x \in \mathbb{R}^N$ and $\underline{\mathbf{Z}}_x \in \mathbb{R}^N$ indicate the upper and lower limits of ZMP inputs, respectively, based on the geometry of the support feet. In the matrix \mathbf{A}_p , the matrix $\mathbf{I}_N \in \mathbb{R}^{N \times N}$ refers to an N size identity matrix and the matrix $\mathbf{S} \in \mathbb{R}^{N \times m}$ represents a selection matrix whose element,

TABLE I: The parameters of CP-MPC and stepping controller used in the simulations and real robot experiments.

CP-MPC	
Parameters	Value
$\mathbf{w}_{\xi,x,y}$	10.0 ($i = 1$), 5.0 ($i = 2 \sim N - 10$), 100.0 ($i = N - 10 \sim N$)
$\mathbf{w}_{p,x,y}$	0.1 ($i = 1$), 10.0 ($i = 2 \sim N - 10$), 0.1 ($i = N - 10 \sim N$)
$\mathbf{w}_{F,x,y}$	0.001
$\mathbf{w}_{\tau,y}$	1.0×10^{-6} ($\Delta z_{min,x} : 0.05$) \rightarrow 0 ($\Delta z_{max,x} : 0.1$)
$\mathbf{w}_{\tau,x}$	1.0×10^{-6} ($\Delta z_{min,y} : 0.04$) \rightarrow 0 ($\Delta z_{max,y} : 0.07$)
\mathbf{K}_d	$50.0 \mathbf{I}_N$
$\mathbf{Z}_x, \bar{\mathbf{Z}}_x [m]$	$(\mathbf{Z}_x^{ref} - 0.09, \mathbf{Z}_x^{ref} + 0.12)$
$\mathbf{Z}_y, \bar{\mathbf{Z}}_y [m]$	$(\mathbf{Z}_y^{ref} - 0.07, \mathbf{Z}_y^{ref} + 0.07)$
$\Delta \mathbf{F}_x, \bar{\Delta} \mathbf{F}_x [m]$	$(-0.2, 0.2)$ w.r.t support foot
$\Delta \mathbf{F}_y, \bar{\Delta} \mathbf{F}_y [m]$	$(-0.1, 0.03)/(-0.03, 0.1)$ w.r.t left/right support foot
$\bar{\boldsymbol{\tau}}_y, \boldsymbol{\tau}_y [N \cdot m]$	$(-15.0, 15.0)$ (Simulation) / $(-7.0, 7.0)$ (Experiment)
Stepping controller	
Parameters	Value
$\mathbf{w}_{f,x,y}$	1000.0
$\mathbf{w}_{b,x,y}$	3000.0
w_γ	1.0
$\underline{f}_{x,y}, \bar{f}_{x,y} [m]$	$(f_{nom,x,y} - 0.05, f_{nom,x,y} + 0.05)$
$\underline{b}_{x,y}, \bar{b}_{x,y} [m]$	$(b_{nom,x,y} - 0.10, b_{nom,x,y} + 0.10)$
$\underline{T}, \bar{T} [s]$	$(T_{nom} - 0.2, T_{nom} + 0.2)$ / $\gamma = e^{\omega T}$

$s_{N,m}$, is 1 or 0. The matrix, \mathbf{S} , activates $\Delta \mathbf{F}_x$ within the time horizon after the current Single Support Phase (SSP). Using $\Delta \mathbf{F}_x$ to relax the ZMP constraint in situations where ZMP control inputs are limited improves the performance of CP control by increasing flexibility in generating ZMP control inputs. The second constraint refers to the limit on the amount of centroidal moment that can be produced by the robot's motion. The vectors $\bar{\boldsymbol{\tau}}_y \in \mathbb{R}^N$ and $\boldsymbol{\tau}_y \in \mathbb{R}^N$ indicate the upper and lower bounds of the centroidal moment, respectively. The last constraint denotes the kinematic constraint of the additional footsteps to prevent singularities and self-collisions between each leg. The vector $\bar{\Delta} \mathbf{F}_x \in \mathbb{R}^m$ and $\Delta \mathbf{F}_x \in \mathbb{R}^m$ refers to the upper and lower bounds of additional footsteps adjustment. The values of weighting parameters and constraints used in the experiments are summarized in Table I.

C. Variable Weighting Parameter for CAM control

The CAM control approaches have been widely utilized in many studies to overcome large disturbances that affect robots. In general, a desired CAM of humanoids is initially generated to overcome external disturbances, but it should be converged to zero in steady-state. This is because there is no need to generate constant CAM for the balancing purpose in steady-state, and furthermore, a constant desired CAM cannot be generated continuously by the joint limits of the robot. The convergence process of desired CAM can be implemented heuristically during a specific time period [20] or under certain conditions [22], [23], [46]. However, this issue is more commonly addressed through optimization methods by implementing a CAM regulation term or damping actions of the CAM change, i.e., centroidal moment, in the cost function [34], [36], [39], [47], [48]. In our case, the convergence process of desired CAM is also addressed through the damping action of the centroidal moment in MPC optimization. However, these approaches commonly suffer from a

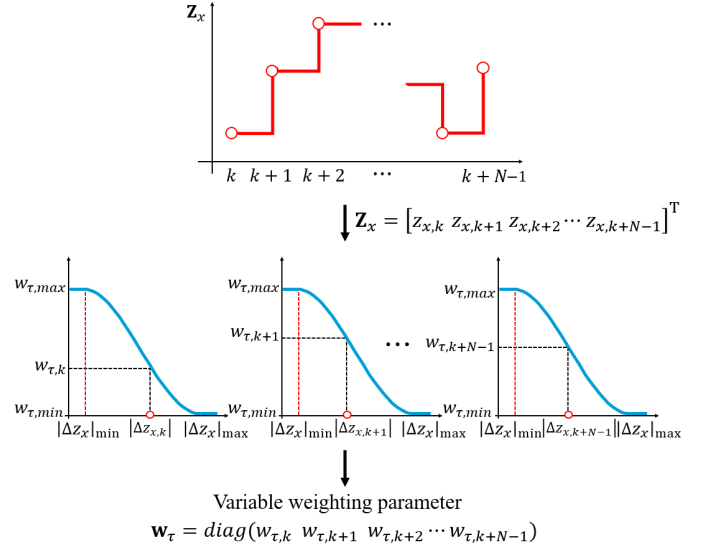


Fig. 3: Decision process of variable weighting parameters in CP-MPC.

trade-off between generating the desired centroidal moment to overcome the disturbance and the term that drives the CAM to zero, which can have a negative impact on the balancing performance.

To address this problem, a novel variable weighting approach based on MPC is proposed. The purpose of this approach is not to compromise the CP control performance when the robot is subjected to large disturbances, by reducing the weighting parameter, \mathbf{w}_τ , to reduce the influence of the damping cost term in (10). This allows the robot to generate more control input $\boldsymbol{\tau}$ in the presence of disturbances, thereby improving balance performance. Furthermore, in the steady-state when the disturbances diminish, the weighting parameter can be increased to dampen the generation of CAM.

Fig. 3 presents the scheme of the decision process of the variable weighting parameters in the x-direction. In Fig. 3, when a significant disturbance is applied to the robot, ZMP control inputs, \mathbf{Z}_x , increase in CP-MPC to control the perturbed CP. Then, weighting parameters, \mathbf{w}_τ , are determined through a one-to-one mapping using cubic function according to the magnitude of the delta ZMP inputs, $|\Delta \mathbf{Z}_x| = |\mathbf{Z}_x - \mathbf{Z}_x^{ref}| \in \mathbb{R}^N$. Note that $\mathbf{Z}_x^{ref} \in \mathbb{R}^N$ represents the reference ZMP trajectory in the x-direction based on the pre-planned footstep. This mapping enables a reduction in \mathbf{w}_τ as the $|\Delta \mathbf{Z}_x|$ for controlling the CP increases. As a result, the damping cost term in (10) becomes less influential, and the centroidal moment, $\boldsymbol{\tau}_y \in \mathbb{R}^N$, is primarily generated to balance the robot against disturbances. The operational principle of this algorithm is based on the observation that the increased ZMP control inputs, \mathbf{Z}_x , indicate that the robot is subjected to a substantial disturbance, thereby requiring more control inputs to accurately track the CP trajectory. Therefore, the capability of CP control can be increased by increasing the generation of another control input, $\boldsymbol{\tau}_y$. The same process is applied in the y-direction, independent of the x-direction.

Finally, the desired centroidal moment, $\boldsymbol{\tau}^{des} = [\boldsymbol{\tau}_y^{des} -$

τ_x^{des} , is integrated to the desired CAM at each time step, $\mathbf{h}^{des} = [h_y^{des} \ h_x^{des}]$, as follows:

$$h_i^{des} = \int \tau_i^{des} dt, \quad i = x, y \quad (12)$$

The desired CAM is controlled by our previously proposed HQP-based CAM controller [23], which prioritizes CAM control first and performs the initial pose return task with secondary priority, resulting in improved CAM control performance. The effectiveness of the variable weighting approach will be validated in Section VI-E.

V. STEPPING CONTROLLER BASED ON CP-MPC

While footstep position adjustment has been extensively studied in MPC approaches [24], [25], [28], [31], [36], optimizing the step time in the MPC formulation is still considered a challenging problem due to its non-convex nature. However, since step time adjustment improves balancing performance compared to adjusting footstep position alone, various methods such as heuristic approaches [24], [44] or optimization based on LIPM assumptions [30], [31], [38], [39], [49] have been conducted in addition to MPC approaches.

In this study, we developed a hierarchical control structure of CP-MPC and the stepping controller, enabling the step time optimization based on MPC variables. Specifically, CP-MPC utilizes ZMP, CAM, and footstep adjustment to track the CP trajectory, while the stepping controller adjusted the footstep position and step time to control the CP offset at the end of step.

A. Overview of the Stepping Controller

In this section, an overview is provided for the adjustment of footstep position and step time to control the CP offset in the stepping controller. Our stepping controller is designed based on the QP optimization proposed by Khadiv et al. [26], [30] using LIPFM based CP end-of-step dynamics. The dynamics of CP end-of-step based on LIPFM can be expressed as follows,

$$\xi_T = \mathbf{f} + \mathbf{b} = (\xi - \mathbf{P}_{ssp})e^{-\omega t}\gamma + \mathbf{P}_{ssp}. \quad (13)$$

In [26], [30], the stepping controller is primarily designed to adjust the next footstep position, $\mathbf{f} = [f_x \ f_y]$, and step time term, $\gamma = e^{\omega T}$, ensuring that the CP offset, $\mathbf{b} = [b_x \ b_y]$, closely aligns with the planned CP offset. The CP offset in LIPM-based walking has been identified as a critical factor that determines the initial point of the exponential growth of the CP in the next step, and has been emphasized in numerous studies [26], [27], [30], [39], [40] as a key factor that affects the walking stability. Based on these concepts, we also adjust the footstep position and step time to control the CP offset.

Fig. 4 presents the overall concept of our approach in the presence of disturbances. When the disturbance is applied to the robot, the CP end-of-step (purple point), ξ'_T , is predicted using (13) to deviate significantly due to the disturbance. In this case, the stepping controller adjusts the footstep position, \mathbf{f} , and the step time term, γ , to control the CP offset, \mathbf{b} , at the end of step. Unlike [26], [30], in our case, \mathbf{f}^{nom} is calculated

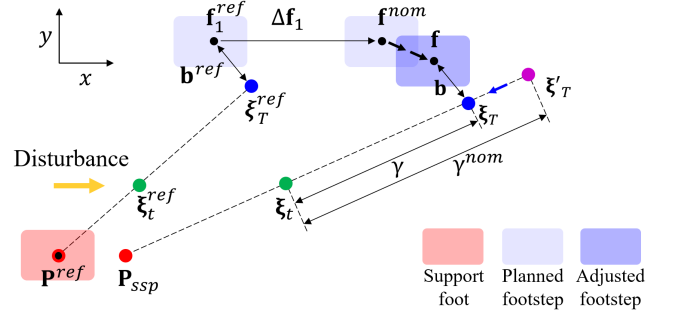


Fig. 4: Schematic representation of the stepping control; In order to control the CP offset, footstep position and step time are adjusted based on CP-end-of-step dynamics.

based on $\Delta \mathbf{f}_1$ planned from CP-MPC, and \mathbf{f} is adjusted to prevent significant deviations from \mathbf{f}^{nom} . Consequently, γ is primarily adjusted to control \mathbf{b} .

B. Parameter Decision based on CP-MPC

This section describes the parameter decision for the nominal values of the next foot position, \mathbf{f} , CP offset, \mathbf{b} , step time term, γ , and CMP parameters, \mathbf{P}_{ssp} , in (13). The nominal footstep position, $\mathbf{f}^{nom} = [f_x^{nom} \ f_y^{nom}]$, is defined as the sum of the reference next footstep position, \mathbf{f}_1^{ref} , determined by the footstep planner and the footstep adjustment, $\Delta \mathbf{f}_1$, optimized by CP-MPC to minimize the CP error over the future horizon, as follows,

$$\mathbf{f}^{nom} = \mathbf{f}_1^{ref} + \Delta \mathbf{f}_1. \quad (14)$$

Here, *nom* and 1 refer to the nominal value and the next footstep, respectively. By incorporating $\Delta \mathbf{f}_1$ into the calculation of \mathbf{f}^{nom} instead of solely relying on \mathbf{f}_1^{ref} , it leads to a reduction in the cost of adjusting \mathbf{f} (see Fig. 4) and consequently reduces the CP offset optimization error.

Next, the nominal CP offset, $\mathbf{b}^{nom} = [b_x^{nom} \ b_y^{nom}]$, is defined as the difference between the reference CP end-of-step, $\xi_T^{ref} = [\xi_{T,x}^{ref} \ \xi_{T,y}^{ref}]$, planned by the walking pattern generator and the reference next footstep position, \mathbf{f}_1^{ref} , to follow the target velocity command,

$$\mathbf{b}^{nom} = \xi_T^{ref} - \mathbf{f}_1^{ref}. \quad (15)$$

The nominal step time term, $\gamma^{nom} = e^{\omega T^{ref}}$, is determined by a pre-defined step time based on the target velocity command.

The CMP parameter, $\mathbf{P}_{ssp} = [p_{ssp,x} \ p_{ssp,y}]$, (as shown in Fig. 4) are calculated based on the average of CP-MPC control inputs (ZMP and centroidal moment control inputs) corresponding to the remaining SSP time within the prediction horizon. The decision to utilize the average CP-MPC control inputs in (13) is based on two considerations. Firstly, by approximating the CP-MPC control inputs as a single point, it becomes possible to reflect the tendencies of where the robot's CMP acts. This approach enables more accurate prediction of the CP end-of-step compared to using a fixed CMP at the center of the support foot or only the CMP control input for the current time step. Secondly, it can improve the overall stability of the stepping controller by smoothing out the noisy input at

the current time step. The equation of the CMP parameter is as follows,

$$\mathbf{P}_{ssp} = \sum_{i=k}^T \frac{\mathbf{z}_i + \boldsymbol{\tau}_i/mg}{T - k + 1} \quad (16)$$

where $\mathbf{z}_i = [z_{x,i} \ z_{y,i}]$ and $\boldsymbol{\tau}_i = [\tau_{y,i} \ -\tau_{x,i}]$ are the ZMP and centroidal moment control input at each time step i , respectively.

C. Formulating a QP problem for Stepping Controller

The QP formulation for adjusting the footstep position and the step time to control the CP offset is as follows.

$$\min_{\mathbf{f}, \gamma, \mathbf{b}} \quad \mathbf{w}_f \|\mathbf{f} - \mathbf{f}^{nom}\|^2 + w_\gamma (\gamma - \gamma^{nom})^2 \quad (17)$$

$$\begin{aligned} & + \mathbf{w}_b \|\mathbf{b} - \mathbf{b}^{nom}\|^2 \\ \text{s. t.} \quad & \underline{\mathbf{f}} \leq \mathbf{f} \leq \bar{\mathbf{f}} \\ & \underline{\gamma} \leq \gamma \leq \bar{\gamma} \\ & \underline{\mathbf{b}} \leq \mathbf{b} \leq \bar{\mathbf{b}} \\ & \mathbf{f} + \mathbf{b} = (\boldsymbol{\xi} - \mathbf{P}_{ssp})e^{-\omega t} \gamma + \mathbf{P}_{ssp} \end{aligned} \quad (18)$$

The cost function in (17) is composed of the footstep position error term, step time error term, and CP offset error term, and each cost is weighted by \mathbf{w}_f , w_γ , and \mathbf{w}_b , respectively. In each of the optimization variables, $\mathbf{f} = [f_x \ f_y]$ represents the next footstep position, γ represents the step time term, and $\mathbf{b} = [b_x \ b_y]$ represents the CP offset. The variable, $\gamma = e^{\omega T}$, is introduced to linearize the equality constraint in (18). The weighting parameter was set primarily to adjust the step time, T , while also enhancing the consistency of \mathbf{f} with the CP-MPC output. To achieve this, we set the smaller weighting value for the step time than the other weighting values as listed in Table. I.

In (18), the inequality constraint is composed of the upper and lower bounds for each optimization variable, and the equality constraint is defined by the LIPFM based CP end-of-step dynamics in (13). The variable, $\boldsymbol{\xi}$, represents the current CP, and the variable, t , represents the elapsed time since the start of the swing phase. The variable, \mathbf{P}_{ssp} , refers to the CMP parameter used in the equality constraint.

D. Characteristic of Our Parameter Selection Approach compared to Previous Methods

In this section, we introduce improvements in our parameter selection approach compared to previous studies [26], [30], [31], [38].

Controlling the CP offset is crucial as it determines the initial velocity of the CP in the next step, thereby significantly affecting walking stability. Previous studies [26], [30], [38] rigorously controlled the CP offset. However, in these studies, the CP offset was derived under the assumption of a constant walking velocity, as follows,

$$b_x^{nom} = \frac{L}{e^{\omega T^{nom}} - 1}, \quad (19)$$

$$b_y^{nom} = (-1)^n \frac{D}{e^{\omega T^{nom}} - 1} - \frac{W}{e^{\omega T^{nom}} - 1}. \quad (20)$$

Here, L represents the step length, D denotes the default step width during walking, and W represents the deviation with respect to the default step width. When n is equal to 1, it indicates the right foot support phase, and when n is equal to 2, it indicates the left foot support phase.

The nominal CP offset in (19) and (20) can be derived simply based on the CP end-of-step dynamics, and a detailed derivation is presented in [30]. However, these derivations include the assumption that the current step and the next step have the same values for L , W , and T^{nom} . Therefore, this assumption is violated when the walking velocity between the current and next steps are different (e.g., walking with different speeds for each step or sudden changes in walking direction). On the contrary, in our approach, while using the same QP formulation (17) as in previous studies, the CP offset is determined from (15), taking into account the variations in walking velocity at each step.

Next, in previous studies [26], [30], [31], [38], it was assumed that the ZMP or CMP is fixed at the center of the support foot ($\mathbf{P}_{ssp} = \mathbf{P}^{ref}$), based on the point foot assumption. However, in most humanoid robots, the foot has a finite size and the ground reaction forces do not act exactly at the center of the support foot. Indeed, the larger the robot's feet, the further the robot's ZMP or CMP can deviate from the center of its support foot. This can potentially violate the point foot assumption on the CP dynamics based on LIPM or LIPFM. Therefore, in this paper, the CMP parameter obtained from CP-MPC is used to consider the behavior of CMP by CP-MPC instead of the point foot assumption.

In Section VI-F, the effectiveness of the parameter selection approach are analyzed through a comparison with the previous methods.

VI. RESULTS OF SIMULATIONS AND EXPERIMENTS

A. System Overview

In this section, a comprehensive system overview for both the simulations and real robot experiments is presented. The humanoid robot, TOCABI, utilized in the simulations and experiments comprises a total of 33 degrees of freedom (DOFs): 16 for the arms, 12 for the legs, 3 for the waist, and 2 for the neck. Its physical dimensions are approximately 1.8 m in height, weighing around 100 kg, and with a foot size of 14 cm \times 30 cm. The upper body actuators are comprised of Parker's BLDC motors and harmonic gears, and the lower body actuators are composed of Kollmorgen's BLDC motors and harmonic gears. The current control of the robot is performed by Elmo Motion Control's Gold Solo Whistle servo controller, and the communication between servo controller and the main PC is achieved via EtherCAT communication. MicroStrain's 3DM-GX5-25 IMU is attached to the pelvis for estimating the global inclination of the robot, and ATI's mini85 F/T sensor is mounted on each foot to measure the contact wrench of the robot. The algorithmic operation and torque command frequency of the robot are set to 2 kHz, and the walking pattern generator and CP-MPC operate at 50 Hz (shown in Fig. 2), due to the high computational load involved, through parallel threads. The walking pattern generator and

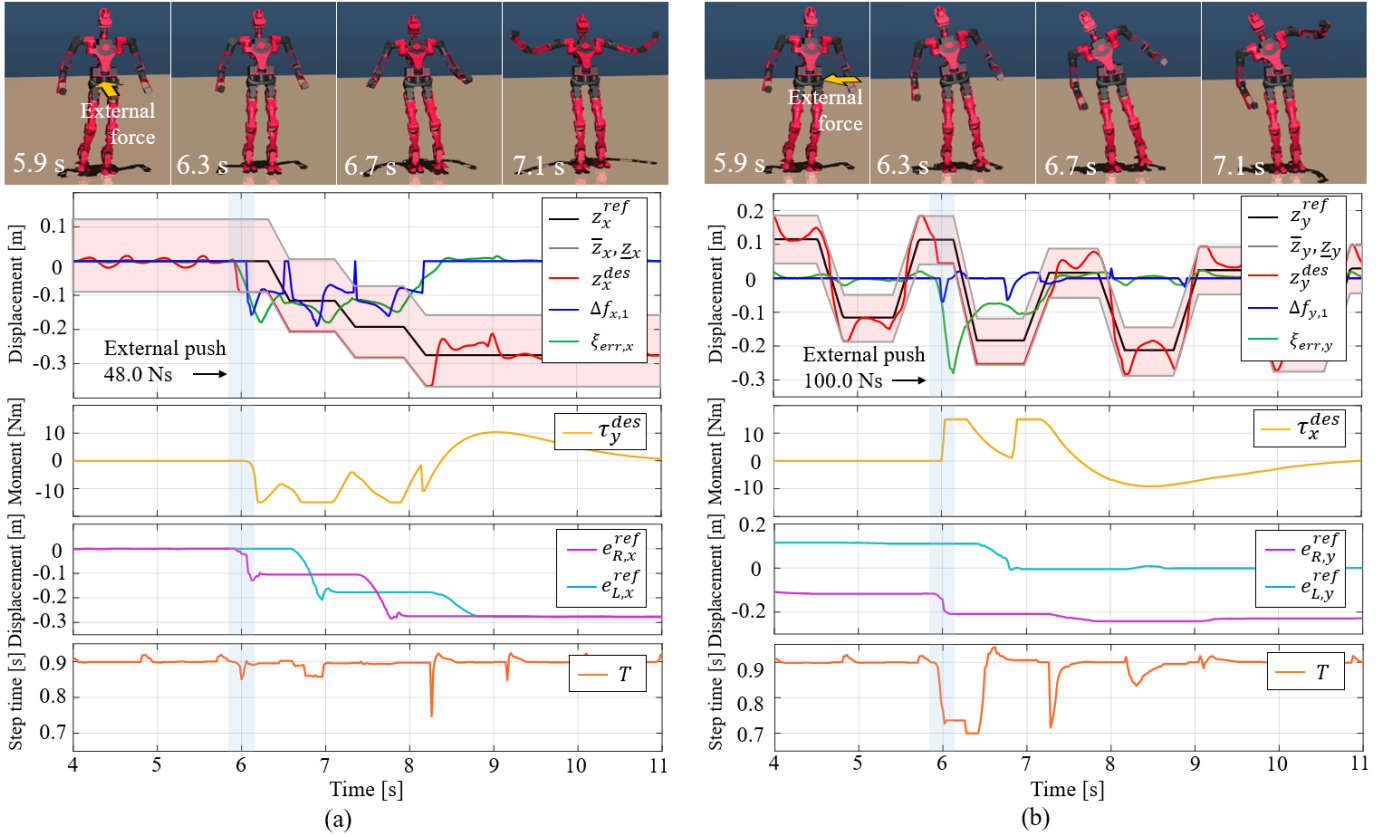


Fig. 5: Simulation results are presented for the robot’s response to external forces applied along both the negative x- and y-directions, shown in (a) and (b) respectively. The second and third rows depict the output of the CP-MPC, while the fourth and fifth rows show the reference foot trajectories and step time by the stepping controller.

CP-MPC have respective MPC time horizons of 2.5 s and 1.5 s. It should be noted that the positive direction of the x-axis represents the robot’s forward direction, while the positive direction of the z-axis is the opposite direction of the gravity vector. The simulator employed in this study is the MuJoCo simulator [50]. The parameters for each controller used in the simulations and experiments of this paper are given in Table. I, and the experimental results videos are available in the supplementary materials.

B. Simulation to Validate Robustness of the Proposed Method under External Forces

Simulations were conducted to evaluate the balancing capability of the robot against external forces using the proposed method. The simulations involved a scenario where the robot walked in the place and external forces are applied to the robot’s pelvis link in the x- and y-directions during an SSP (left foot support). The step duration was configured to consist of an SSP of 0.6 s and a DSP of 0.3 s. Furthermore, adjustments of the footstep position and step time are not allowed 0.1 s before the end of SSP to prevent jerky motions in the swing leg.

In the first simulation, a step external force of 240 N was applied to the robot’s pelvis in the negative x-direction for 0.2 s. Fig. 5(a) shows snapshots and data of the robot’s response to the external force. The sequence of the snapshot

provides a visualization of the overall balancing process. The robot maintains balance by employing ZMP control using the supporting legs (ankle strategy), CAM control using the upper body (hip strategy), and performing back steps (stepping strategy).

The graph in Fig. 5(a) represents the outputs of the CP-MPC and stepping controller in the x-direction. At approximately 5.9 s, the robot’s CP was pushed backward, causing the CP error (green line), $\xi_{err,x}$, to increase in the negative x-direction due to the external force. To reduce the CP error, the desired ZMP (red line), z_x^{des} , is generated by the CP-MPC. Despite the attempts to reduce the CP error through the desired ZMP, it remained high due to the significant external force and the ZMP constraint of -9 cm. As a result, the CP error increased and reached up to -17.9 cm. Then, footstep adjustment (blue line), $\Delta f_{x,1}$, was generated to relax the ZMP constraint and the desired centroidal moment (yellow line), τ_y^{des} , was also generated to reduce the CP error additionally. The desired ZMP was generated up to the relaxed ZMP constraint until approximately 8.2 s, while the centroidal moment was generated up to the limit of -15 Nm until approximately 7.9 s. Meanwhile, the stepping controller performed a total of four back-steps (magenta and cyan line) based on $\Delta f_{x,1}$, moving approximately -27.5 cm in conjunction with an optimal step time (orange line), T . As a result, the CP error is reduced to approximately zero, and the

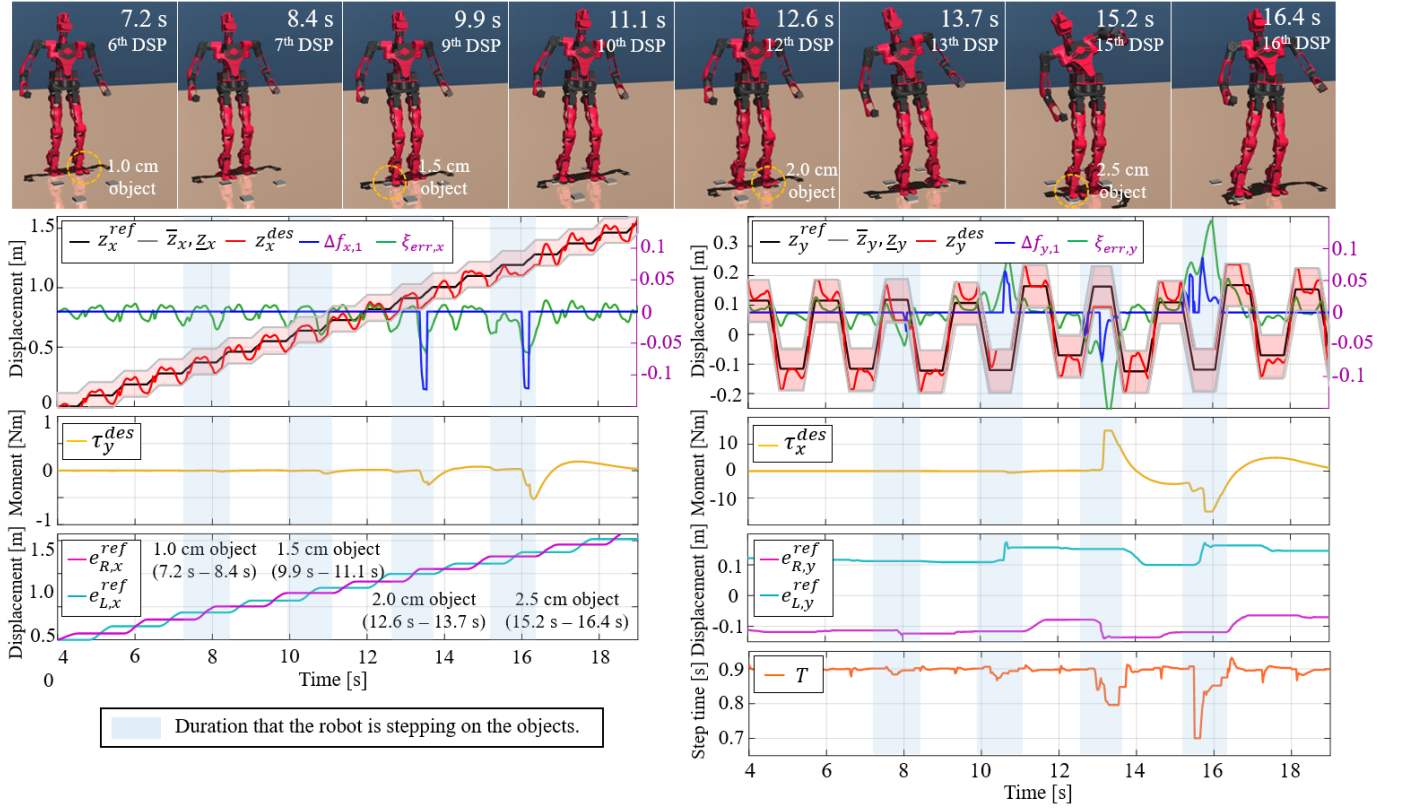


Fig. 6: Simulation results are presented for the robot’s forward walking while overcoming four unexpected objects, with snapshots and output data provided. The second and third rows represent the output of the CP-MPC, while the fourth and fifth rows show the reference foot trajectories and step time by the stepping controller.

robot maintains a balance against the external force.

In the following simulation, a step external force of 500 N was applied to the robot’s pelvis in the negative y-direction for 0.2 s. Fig. 5(b) presents snapshots and y-direction data of the robot’s response to the external force. Similar to the previous simulation, the robot maintained balance by stepping in the direction of the external force while performing ZMP control and CAM control.

Fig. 5(b) represents the robot’s data, including the CP-MPC and stepping controllers’ y-direction outputs. At approximately 5.9 s, the external force was applied to the robot in the negative y-direction, leading to a significant deviation in the CP error (green line), $\xi_{err,y}$. The CP-MPC attempted to decrease the increasing CP error by generating the desired ZMP up to the ZMP constraint. However, the CP error could not be reduced due to the significant external force. At approximately 6 s, footstep adjustment of -7 cm (blue line), $\Delta f_{y,1}$, was generated to relax the ZMP constraint, and 15 Nm of the desired centroidal moment (yellow line), τ_x^{des} , was also generated to reduce the CP error. Based on the generated $\Delta f_{y,1}$, the stepping controller adjusted the foot trajectory (magenta and cyan line) and reduced the step time (orange line), T , to allow for stepping at approximately 6.1 s. After the stepping, the desired ZMP and the centroidal moment were continuously generated up to their respective limits until approximately 7.2 s to overcome disturbances. Subsequently, continuous CP control using each strategy reduced the CP error from

approximately -28 cm initially, gradually decreasing until the robot was able to maintain balance against external forces.

C. Simulation to Validate Robustness of the Proposed Method on Uneven Terrain

Although the robustness of the proposed method was validated against external forces, it is imperative to ensure its ability to maintain balance against disturbances arising from uneven terrain. Therefore, in this simulation, the robot walks over objects placed on the ground, demonstrating the performance of the algorithm on uneven terrain. Four objects, each with a length and width of 5 cm, were positioned in front of the robot with a distance of 30 cm between them. To make the robot step on each object alternately, two objects were placed on the left and two on the right with respect to the robot’s center. The thickness of the objects ranged from 1.0 cm to 2.5 cm with an increase of 0.5 cm. The robot walked a distance of 2.0 m with a step length of 0.1 m, and the step duration consisted of 0.6 s of SSP and 0.3 s of DSP. In the second row of Fig. 6, the left y-axis of the graph represents the displacements of variables related to ZMP. Conversely, the right y-axis, indicated by the purple color, displays the CP error, ξ_{err} , and footstep adjustment, Δf_1 . This arrangement is intended to enhance the visibility of variations in CP error and footstep adjustment, enabling a more detailed analysis of their changes.

Fig. 6 shows simulation snapshots and the corresponding output data. The snapshots provide a reaction of the robot to each object before and after stepping on it, from the beginning of the DSP to the end of the next DSP. In the snapshots, the robot was able to navigate forward while stepping on the objects in its path. The first and second objects were overcome using ZMP and stepping control (ankle and stepping strategies). For the third and fourth objects, CAM control (hip strategy) was additionally employed to navigate past them. The analysis of this process is explained based on the data presented in the graphs.

First, at approximately 7.2 s, which is the start of the 6th DSP, the robot steps on the object with a thickness of 1.0 cm diagonally in the y-direction, causing external disturbance. To reduce the CP error (green line) from the disturbance, the desired ZMP (red line) was first generated in the x- and y-directions, and a footstep adjustment $\Delta f_{y,1}$ of -2.9 cm (blue line) was generated at approximately 8.1 s. Due to the narrower range of ZMP constraint in the y-direction compared to the x-direction, $\Delta f_{y,1}$ was generated somewhat faster. As a result, the swing foot position (cyan and magenta line) was adjusted with the ZMP control, allowing the robot to overcome the external disturbance.

At the start of the 9th DSP, approximately 9.9 s, the robot encountered the 1.5 cm object. To overcome the resulting disturbance, the CP-MPC generated $\Delta f_{y,1}$ of 6.5 cm at approximately 10.6 s. Compared to the first disturbance, the robot overcame disturbances by employing a more proactive stepping control in the y-direction, including adjusting the footstep and step time (orange line), T .

Next, at the start of the 12th DSP, approximately 12.6 s, the robot stepped on the 2 cm object. To alleviate the CP errors caused by object disturbance, the desired ZMP was generated up to the constraint in both the x- and y-directions. Additionally, $\Delta f_{y,1}$ of -7.6 cm was generated at approximately 13.1 s and $\Delta f_{x,1}$ of -12.2 cm was also generated at 13.4 s. Notably, the large CP error in the y-direction led to a maximal x-axis centroidal moment, τ_x^{des} , of 15 Nm. In conclusion, the robot was able to overcome disturbances by adjusting step position and time to a greater extent than in the second stepping case, while also implementing centroidal moment control.

Finally, at the start of the 15th DSP, approximately 15.2 s, the robot stepped on the thickest object of 2.5 cm among the objects. The desired ZMP in the x- and y-direction were generated in two steps up to each ZMP constraint compared to the third balancing case. $\Delta f_{y,1}$ was generated up to 8.6 cm at approximately 15.7 s, and $\Delta f_{x,1}$ was generated up to -11.9 cm at approximately 16.1 s. The centroidal moment in the x-direction was also generated up to the constraint due to a significant disturbance. With footstep position adjustment, step time was also reduced by up to 0.7 s, allowing the robot to overcome the disturbance. On the other hand, only a small amount of the centroidal moment, τ_y^{des} , in the y-direction was generated.

In conclusion, this simulation showed that appropriate strategies were executed to mitigate disturbances of various magnitudes caused by uneven terrain, and the graph data

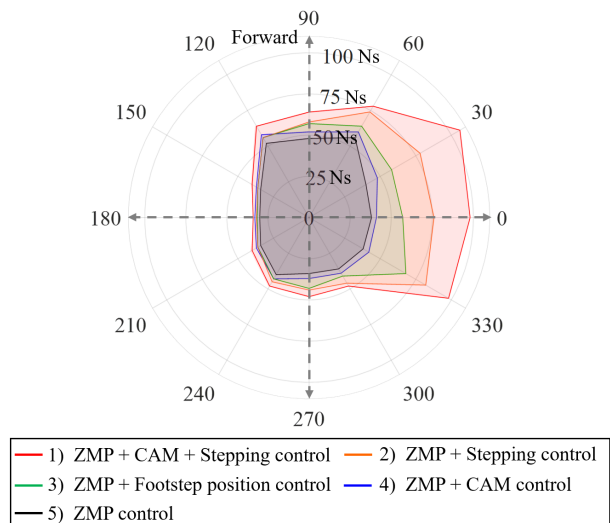


Fig. 7: Comparisons of the maximum endurable impulse between combinations of strategies.

provided clear evidence of the effectiveness of these strategies.

D. Simulation to Evaluate Balancing Performance based on the Different Combinations of Each Balance Strategy

Comparative simulations were conducted to evaluate how the balancing performance varies based on different combinations of balancing strategies in response to disturbances. Presented below is a summary of the implementation methods employed to combine each strategy.

- Method 2) is composed of a combination of ZMP control and stepping control (footstep position and step time adjustment), excluding the CAM control. To achieve this, the prediction model of CP-MPC in (6) was modified to include LIPM dynamics but not LIPFM, and all terms related to the centroidal moment, τ , in (10) and (11) were excluded. All other controllers were kept the same.
- Method 3) has the same structure as method 2), but it does not consider step time adjustment in the stepping controller. Therefore, only the next footstep position, f , is adjusted in the stepping controller without modifying the step time, T .
- Method 4) is a combination of ZMP control and CAM control, excluding the stepping control. To achieve this, all terms related to ΔF in (10) and (11) were excluded, and the stepping controller was also excluded.
- Method 5) only performs ZMP control. All terms related to τ and ΔF in (10) and (11) were excluded, as well as the stepping controller.

In order to analyze the robustness of each method against disturbances from various directions, the maximum external impulse that the robot could withstand was analyzed by varying the direction of the external force in increments of 30 deg. Similar to previous simulations, an external force was applied to the pelvis of the robot for 0.2 s while the robot walked in place. In Fig. 7, the maximum external impulse that the robot can withstand is represented by the form of

a polygon, which is referred to as the disturbance polygon (DP) in this paper. The direction of the external force vector starts from the robot and points outward, and a force of 90 deg represents a force that is directed from back to front (+x-axis).

As expected, method 5), which only tracks the desired ZMP, exhibited the lowest balancing performance compared to other methods. This is because CP control is achieved only through ZMP control, and ZMP control performance is limited within the support polygon. Method 4), which tracks the desired ZMP and centroidal moment, extended the range of the control input that controls CP beyond the support polygon compared to method 5), resulting in a 9.9 % increase in the average maximum external impulses that the robot can withstand. Method 3), which tracks the desired ZMP and adjusts the footstep position, significantly expands the maximum endurable impulses compared to 4) and 5) at 0, 30, and 330 degrees, where the support area can be greatly widened through stepping. In cases where the stepping distance is limited due to the self-collision, i.e. near 180 degrees, the contribution of the footstep position adjustment to the robustness decreases compared to the other directions and becomes similar to that of method 4). In method 2), which simultaneously tracks the desired ZMP and adjusts footstep position and step time, it was possible to adjust the footstep position more quickly in response to disturbances compared to method 3). In particular, this led to a noticeable improvement in balancing performance, especially at 0, 30, and 330 degrees. Additionally, the average maximum external impulses that the robot could withstand increased by approximately 16.3 % compared to method 3). Our proposed method, which combines all strategies, exhibited superior balancing performance across all directions compared to other sub-combinations. This is because all limbs of the robot (supporting leg, upper body, and swing leg) participated in CP control in parallel through three balance strategies (ankle, hip, and stepping strategies). As a result, our method led to an increase of 19.0 %, 36.2 %, 55.7 %, and 71.1 % in the average maximum external impulses that the robot could withstand compared to methods 2), 3), 4), and 5), respectively.

E. Simulation to Validate the Effectiveness of the Variable Weighting Method

In order to evaluate the effectiveness of the proposed variable weighting method in the presence of disturbance, a comparative simulation with the constant weighting method was performed. The simulation setup was identical to that in Sec VI-B, where an external force was applied to the robot's pelvis in the negative x-direction during walking in place. In this simulation, only the effects of external forces in the x-direction were analyzed, as the results in the y-direction were found to be similar. Fig. 8 presents the results of comparing the performance of the two methods. The first graph shows the relationship between CP error and the magnitude of the current delta ZMP, $|\Delta z_x|$, indicating an increasing trend in delta ZMP as the CP error increases. The delta ZMP refers to the additional ZMP input needed to control the CP error, which is calculated as the difference between the desired ZMP

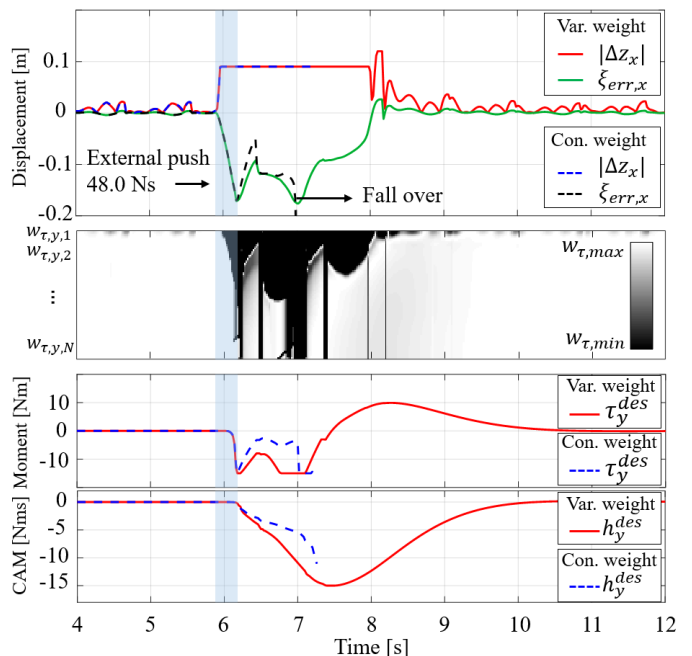


Fig. 8: The impact of variable weight parameters on CAM generation and resulting balancing performance.

and the reference ZMP, as explained in Section IV-C. The second graph shows how the weighting parameter varies with the series of the delta ZMP inputs, $|\Delta \mathbf{Z}_x|$, using a color-map. The third and fourth graphs compare the centroidal moment and CAM generated by each weighting method.

In the first graph of Fig. 8, both methods exhibit an increase in CP error (green and black dotted line) when the external force is applied to the robot at approximately 5.9 s. As a result, the magnitude of delta ZMP input (red and blue dotted line) also increases. Note that the weighting parameters changes according to N series of delta ZMP inputs, but the graph depicts only the first element of delta ZMP inputs to show the overall behavior with respect to CP error.

The second graph depicts the time sequence of N weighting parameters based on the magnitude of N series of delta ZMP inputs, $|\Delta \mathbf{Z}_x|$, over the time horizon (vertical axis). In the variable weighting method, the graph appears white when no disturbance is applied to the robot. However, as the delta ZMP increases due to disturbances after approximately 6 s, the weighting parameters of the CAM damping cost decrease, causing the color-map to turn dark. In contrast, the constant weighting method always has a constant weighting value regardless of delta ZMP inputs.

As evident from the third and fourth graphs, the difference between the two methods significantly impacts the generation τ_y^{des} for disturbances. As a result, it directly affects the desired CAM, h_y^{des} , which is generated by integrating τ_y^{des} . Although the delta ZMP was almost the same (as shown in the graph of the first row), using constant weighting method resulted in the insufficient generation of CAM compared to variable weighting method. This led to the robot falling over after approximately 7.0 s when the constant weighting is used.

Similar to the simulation in VI-B, the performance of

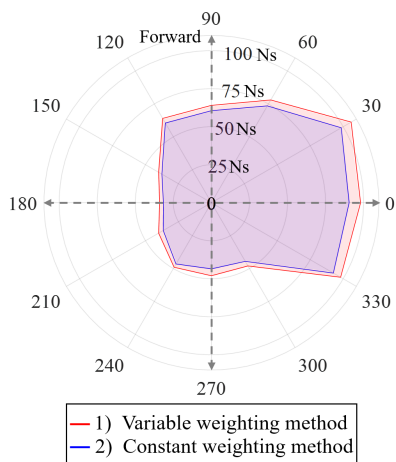


Fig. 9: Comparisons of the maximum endurable impulse between variable and constant weighting method.

TABLE II: Analysis of CP offset errors and CP tracking errors according to the selection of nominal CP offset, \mathbf{b}^{nom} .

Scenario	Method	RMS error [cm]			
		ξ_x	ξ_y	b_x	b_y
(a) Forward and backward walking	Constant velocity assumption [26,30]	1.12	3.56	3.55	7.60
	Our approach	0.76	0.89	1.65	1.46
(b) Lateral walking	Constant velocity assumption [26,30]	0.58	4.78	2.12	9.73
	Our approach	0.39	1.29	0.88	1.94

the variable weighting method was tested against various directions of disturbances, and the results were illustrated in Fig. 9. The use of the variable weighting method led to a 7.2 % increase in the average maximum external impulses that the robot can withstand compared to the constant weighting method.

F. Simulation to evaluate walking performance based on different parameter selections of the stepping controller

In this section, simulations were conducted to analyze the impact of parameter selection in the stepping controller on walking stability. Specifically, the CP tracking error, ξ_{err} , and CP offset error, \mathbf{b}_{err} , were analyzed according to the two parameters (nominal CP offset, \mathbf{b}^{nom} , and CMP parameter, \mathbf{P}_{ssp}). Fig. 10 illustrates the walking scenarios conducted in this simulation. Fig. 10(a) represents forward and backward walking with step length L , and in this case, the deviation of the step width W is zero during walking. Fig. 10(b) represents the lateral walking with step width deviation W , where the default step width D is 20.5 cm. Additionally, in this case, the step length L is zero during walking.

First, in order to analyze the effects of the nominal CP offset, \mathbf{b}^{nom} , on walking stability, simulations were conducted in two walking scenarios depicted in Fig. 10. For comparative simulations, an analytical CP offset calculation method proposed in [26], [30] was adopted. Here, both methods used the CMP parameter, \mathbf{P}_{ssp} , calculated by (16). Table II shows the root mean square (RMS) error of the CP offset and the CP tracking when different nominal CP offsets are selected in

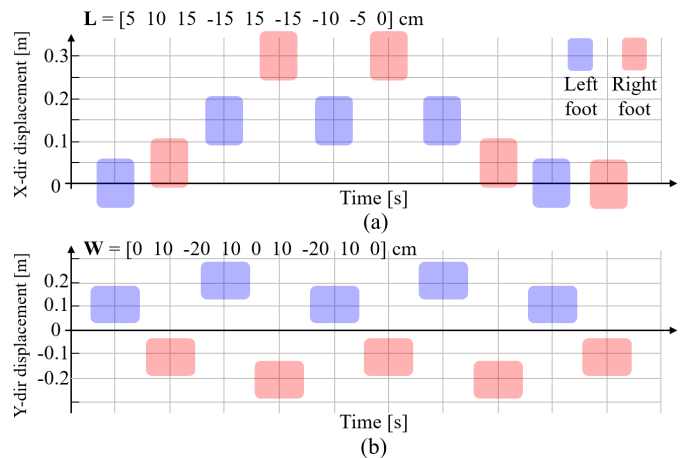


Fig. 10: The planned footstep placement used in the simulation of Section VI-F (a) forward and backward walking at various speeds in the x-direction. (b) lateral walking while the robot doesn't move in the x-direction.

TABLE III: Analysis of CP offset errors and CP tracking errors according to the selection of CMP parameter, \mathbf{P}_{ssp} .

Scenario	Method	RMS error [cm]			
		ξ_x	ξ_y	b_x	b_y
(a) Forward and backward walking	Point foot assumption [26,30,31]	0.96	1.22	1.93	2.04
	Our approach	0.76	0.89	1.65	1.46
(b) Lateral walking	Point foot assumption [26,30,31]	0.56	1.56	0.96	2.79
	Our approach	0.39	1.29	0.88	1.94

each scenario. When adopting \mathbf{b}^{nom} calculated using (19) and (20) proposed in [26], [30], substantial CP tracking errors and CP offset errors were observed in both scenarios (a) and (b) compared to our method. As mentioned in Section V-D, this method assumes that both L in (19) and W in (20) remain constant for the current and the next step. However, as shown in Fig. 10, this assumption is violated in scenario (a) where L changes at each step, or in scenario (b) where W changes at each step. As a result, unintended CP velocity is induced at the beginning of each step, leading to a deterioration in walking stability. This causes significant CP tracking errors and CP offset errors during walking. When our method is used, the CP offset is calculated based on (15) according to the walking velocity command without the constant walking velocity assumption. Consequently, the CP offset is controlled to follow the walking velocity command, allowing the robot to minimize CP tracking error and start the next step with a small CP error, thereby maintaining walking stability.

Next, simulations were performed to analyze the impact of CMP parameter, \mathbf{P}_{ssp} , on walking stability for both scenarios (a) and (b). Here, our CP offset calculation method (15) was used. For the comparison simulations, the CMP parameter [26], [30], [31] that assumed the point foot was compared with our method, and the results are presented in Table III. In both scenarios (a) and (b), the point foot assumption resulted in larger errors compared to our method. The reason is that the point foot assumption fails to accurately reflect the CMP position acting on a robot with large feet, thus ignoring the

causal relationship between the predicted CP end-of-step and the CMP, which operates based on LIPFM dynamics. As a result, the CP end-of-step is inaccurately predicted, and CP offset control based on this CP end-of-step leads to a deterioration of walking stability during walking. On the other hand, our approach calculates the CMP parameter based on the control inputs of CP-MPC in (16), which accurately reflects the robot's CMP compared to the point foot assumption, enabling accurate prediction of CP end-of-step.

In conclusion, it is important to adopt appropriate parameters for the stepping controller to enhance the overall stability of walking.

G. Simulation to Compare Robustness against Disturbances with QP-based CP controller [39]

In this section, simulations were conducted to compare the robustness against disturbances between the proposed method and state-of-the-art QP-based CP controller [39]. For the comparative simulations, the algorithm proposed by [39] was implemented in our walking control framework (see Fig. 2). In the implemented algorithm, the QP-based CP controller replaced our CP-MPC and stepping controller, while all other controllers and planners, including the ZMP controller, CAM controller, and walking pattern generator described in Section III, remained unchanged.

The reasons for selecting the QP-based method [39] as a suitable comparison for our method are the followings. First, our method and the QP-based method are based on the same CP dynamics of the LIPFM and integrate ankle, hip, and stepping strategies that include step time optimization. Second, the QP-based method is considered state-of-the-art research in this field.

While the QP-based method only considers the robot's CP for the current step duration, our CP-MPC takes into account not only the current states but also the future constraints and future states of the robot. The QP formulation proposed by [39] is defined as follows:

$$\min_{\mathbf{f}, \gamma, \boldsymbol{\tau}, \mathbf{b}} \quad \mathbf{w}_f \|\mathbf{f}_{err}\|^2 + w_\gamma (\gamma_{err})^2 + \mathbf{w}_\tau \|\boldsymbol{\tau} + \mathbf{K}_d \mathbf{h}\|^2 + \mathbf{w}_b \|\mathbf{b}_{err}\|^2 \quad (21)$$

$$\text{s. t.} \quad \mathbf{f}_{err} + \mathbf{b}_{err} - \boldsymbol{\xi}^{ref} e^{-\omega t} \gamma_{err} - (1 - e^{-\omega t} \gamma') \frac{\boldsymbol{\tau}_{err}}{mg} = (\boldsymbol{\xi}_{err} - \Delta \mathbf{z}) e^{-\omega t} \gamma_{err} + \Delta \mathbf{z} \quad (22)$$

where the subscript, *err*, signifies the difference between the optimization variables and the pre-designed nominal variables. The delta ZMP, $\Delta \mathbf{z} = [\Delta z_x \ \Delta z_y]$, denotes the difference between the desired ZMP for controlling the CP and the pre-designed reference ZMP. The cost function (21) comprises the step position error term, step time error term, damping term of the CAM, and CP offset error term. The equality constraint in (22) is derived from the error dynamics of the CP end-of-step dynamics in LIPFM. Detailed derivation and explanations for each equation are provided in [39].

The QP formulation in (21) and (22) addresses the ankle strategy through delta ZMP, $\Delta \mathbf{z} \in \mathbb{R}^2$, the hip strategy through centroidal moment, $\boldsymbol{\tau} \in \mathbb{R}^2$, and the stepping strategy through

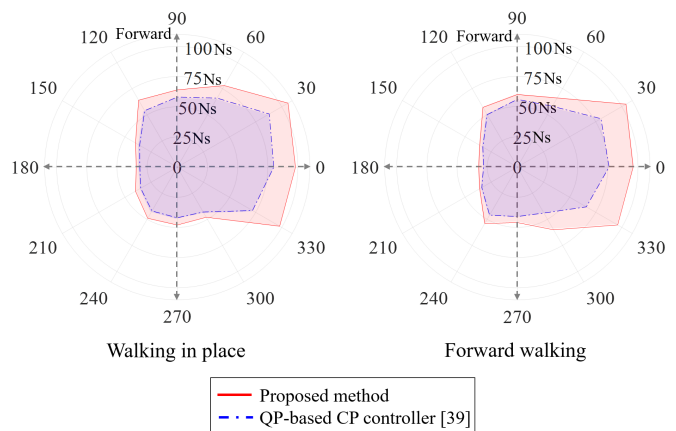


Fig. 11: Comparisons of the maximum endurable impulse during walking between the proposed method and QP-based CP controller [39].

footstep position, $\mathbf{f} \in \mathbb{R}^2$, and step time, γ . However, due to the variable coupling between $\Delta \mathbf{z}$ and γ , as well as between γ and $\boldsymbol{\tau}$, the original equation of (22) resulted in non-linear constraint. To address this issue in [39], $\Delta \mathbf{z}$ is considered as a constant using the pre-computed value from the instantaneous CP controller proposed in [40] without optimization. Furthermore, to avoid variable coupling between $\boldsymbol{\tau}$ and γ , a constant γ' was used, which corresponds to the γ from the previous control cycle. In contrast, our approach optimizes ZMP, centroidal moment, and footstep position simultaneously using CP-MPC, and the step time is separately optimized in the stepping controller without any constant assumptions.

Simulations were conducted to compare the robustness of two algorithms against external forces. The robot was applied to external forces during walking in place and forward walking, and the maximum impulse that the robot could withstand was analyzed using DP. The weighting parameter in (21) was the same as that used in [39]. Fig. 11 shows the DP obtained when using both methods. Overall, our method exhibited more robust balancing performance, especially at 0, 30, and 330 degrees, compared to the QP-based method. The overall difference in balancing performance may first be attributed to the ankle strategy. In [39], the desired ZMP for instantaneous CP control is calculated as follows,

$$\begin{aligned} \mathbf{z}^{des} &= \mathbf{z}^{ref} + \Delta \mathbf{z} \\ &= \mathbf{z}^{ref} - \frac{e^{\omega(T-t)}}{1 - e^{\omega(T-t)}} \boldsymbol{\xi}_{err}. \end{aligned} \quad (23)$$

However, in (23), since the CP control feedback gain is determined based on the remaining step time ($T - t$), the CP control performance cannot be increased as needed. Next, as analyzed in Section VI-B, stepping control was the most helpful in withstanding external forces at 0, 30, and 330 degrees. In our method, footstep position is adjusted based on the ZMP constraint, while step time is adjusted based on CP-MPC outputs, and is independent of the execution order of each balancing strategy. However, in the QP-based method, the ankle, hip, and stepping strategies are executed

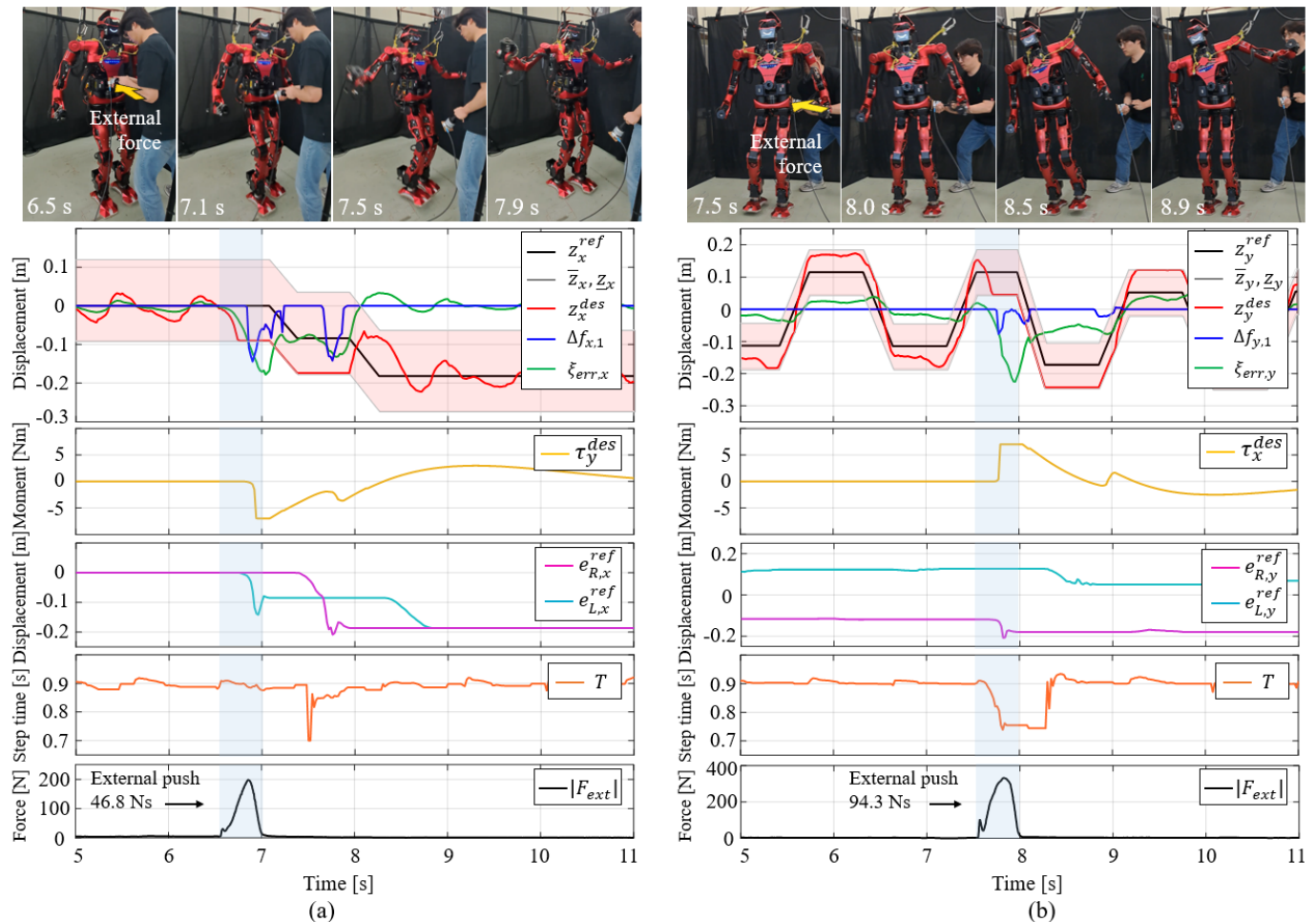


Fig. 12: Experimental results are presented for the robot’s response to external forces applied along both the negative x- and y-directions, with snapshots and output data shown in (a) and (b) respectively.

sequentially according to the magnitude of the CP error, and the stepping control is performed in the final stage. Therefore, the response to disturbances through stepping control was slower compared to our method. The start time of the stepping control for each method is measured 10 times when the robot was subjected to the maximum external impulse that our method could withstand at 0, 30, and 330 degrees (in Fig. 11). Our method on average outpaced the QP-based method by 0.078 s, 0.086 s, and 0.084 s for each direction, respectively. Considering the SSP time (0.6 s), this means that stepping control in our method was performed 13%, 14.3%, and 14% faster than the QP-based method, respectively. In conclusion, when using our method compared to the QP-based method [39], the average maximum external impulses that robot could withstand increased by 21.0 % for walking in place and 26.1 % for forward walking. The video of these comparison simulations can be found in the supplementary material.

H. Real Robot Experiment to Validate Robustness of the Proposed Method under External Forces

Experiments were conducted where the robot was subjected to external forces in both x- and y-directions during walking in place, replicating the scenarios in the simulation presented

in Section VI-B. The external force was applied to the robot directly by a human using a tool equipped with an F/T sensor. The magnitude of the impulse applied to the robot was measured by the F/T sensor on the tool. The step duration includes an SSP of 0.6 s and a DSP of 0.3 s which is consistent with the simulation setup. The control parameters used in both the simulation and experiment are identical, except for the constraints of the centroidal moment (as shown in Table. I). The difference in centroidal moment constraints is due to the conservative assignment of upper body joint position and velocity limits in the real robot experiments compared to the simulation. Consequently, this implies that if the low-level control of the real robot is already adjusted to suit the hardware, there is no need for tuning of control parameters during sim-to-real implementation.

In the first experiment, the robot was subjected to an external push of 46.8 Ns in the negative x-direction while in the right foot support. The snapshots of the experiment and the corresponding experimental data are shown in Fig. 12(a). The snapshot provides a visual representation of how the robot maintained its balance in response to the external force. In a manner similar to the simulation presented in Section VI-B, the robot successfully overcome the external force by combin-

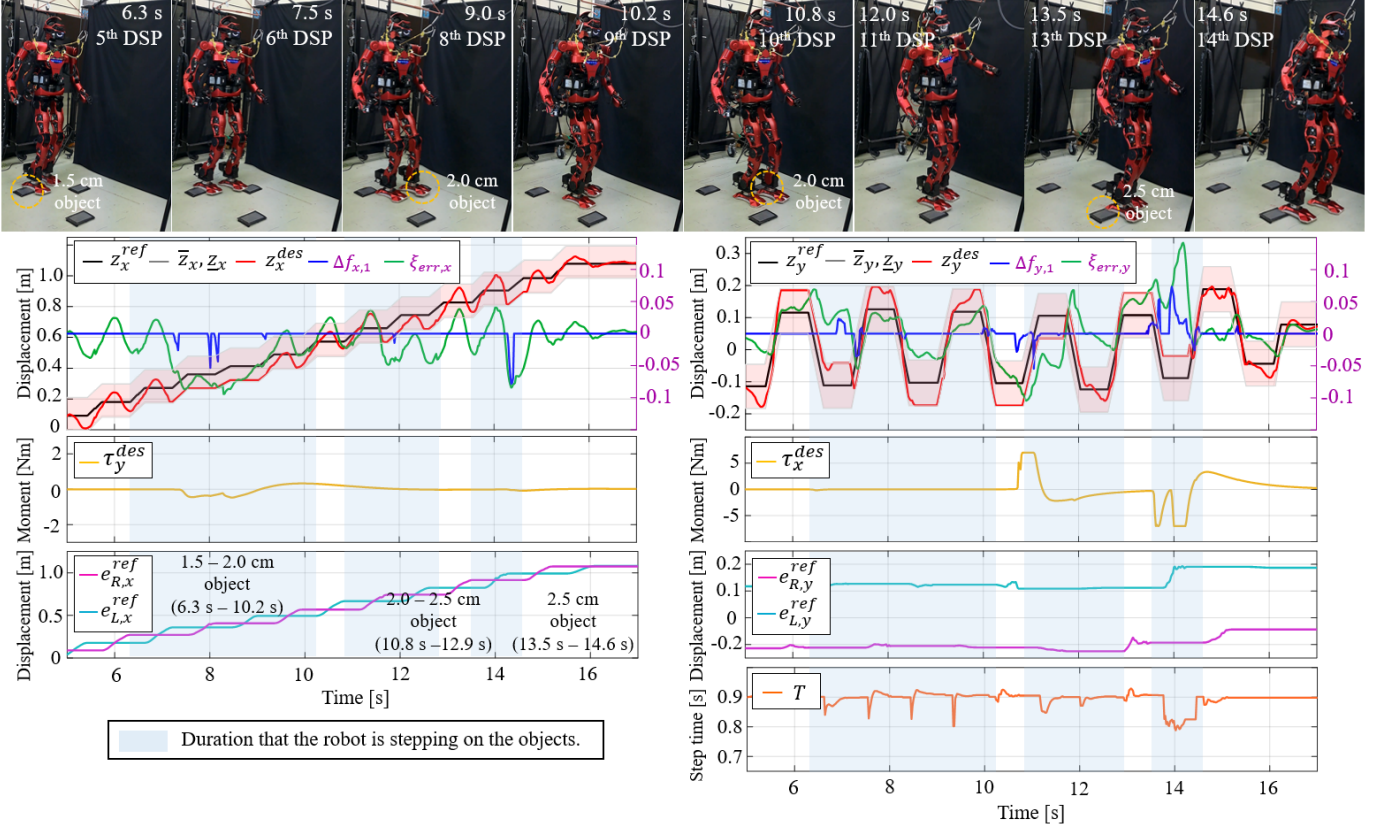


Fig. 13: Experimental results are presented for the robot's forward walking while overcoming three unexpected objects, with snapshots and output data provided.

ing CAM control utilizing the upper body, ZMP control using the supporting leg, and back-steps control. At approximately 6.5 s, when the external force is applied to the robot, the CP error (green line), $\xi_{err,x}$, increases in the negative x-direction, and the desired ZMP (red line), z_x^{des} , is rapidly generated in the direction to reduce the CP error in the CP-MPC. The desired ZMP is then constrained by the ZMP constraint of -9 cm, and CP-MPC generates a footstep adjustment (blue line), $\Delta f_{x,1}$, with a peak value of approximately -14.4 cm to relax the ZMP constraint at approximately 6.9 s. Additionally, the desired centroidal moment (yellow line), τ_y^{des} , is generated up to -7.0 Nm to further reduce the CP error at approximately 6.95 s. Despite these efforts, the robot was unable to overcome the strong disturbance in a single step. As a result, the CP-MPC continuously generated footstep adjustment to reduce the CP error while the desired ZMP was generated up to the constraint until approximately 7.9 s. In conclusion, a total of two back-step controls (magenta and cyan lines) were performed, involving a movement of approximately -18.6 cm, along with step time optimization (orange line), T , and the robot maintained its balance. In contrast, when the QP-based method proposed in [39] was used in the experiment, despite an external push of 38.7 Ns in the negative x-direction, the CP of the robot could not be recovered and the robot lost its balance.

In the following experiment, the robot was subjected to an external push of 94.3 Ns in the negative y-direction during

left foot support. The corresponding experimental data and snapshots are presented in Fig. 12(b). Similar to the previous experiment, the robot maintained its balance through integrated control strategies, including ZMP control using the supporting leg, CAM control using the upper body, and stepping control. At approximately 7.5 s, the external force caused significant perturbation to the robot's CP, resulting in an increase in CP error, $\xi_{err,y}$, in the negative y-direction. To reduce the CP error, the desired ZMP, z_y^{des} , was generated up to the ZMP constraint at approximately 7.7 s. The CP-MPC then generated a footstep adjustment, $\Delta f_{y,1}$, of approximately -7.4 cm and a maximum centroidal moment, τ_x^{des} , of 7 Nm. Additionally, the stepping controller decreased the step time, T , to 0.74 s. Subsequently, the desired ZMP was continuously generated up to the ZMP constraint to reduce the CP error until approximately 9 s. However, centroidal moment or footstep adjustment was reduced after 8.1 s, and CP control was handled mainly through desired ZMP control. Finally, the robot maintained balance against external forces within two steps. On the other hand, when using the QP-based method [39], the robot could not withstand an external force of approximately 75.43 Ns and lost balance. Overall, the magnitude of external impulses applied to the robot was similar to those in the simulation, although it was hard to make them identical by human.

I. Real Robot Experiment to Validate Robustness of the Proposed Method on Uneven Terrain

To validate the robustness of the proposed method against disturbances caused by uneven terrain, a real robot experiment was conducted where the robot walked over objects placed on the ground. In a scenario similar to the simulation in Section VI-C, three objects, each with a length of 15 cm and width of 20 cm, were placed in front of the robot. The distance between the first and second objects was 25 cm, and the distance between the second and third objects was 40 cm. The objects were placed alternately on the left and right sides of the robot's center. The thickness of the objects ranged from 1.5 cm to 2.5 cm in increments of 0.5 cm, similar to the scenario in Section VI-C. The robot walked a distance of 1.3 m with a step length of 0.1 m, and the walking duration consisted of 0.6 s of SSP and 0.3 s of DSP. In the second row of Fig. 13, the left y-axis represents the displacements of variables associated with the ZMP. In contrast, the right y-axis, denoted by the purple color, displays the CP error, ξ_{err} , and footstep adjustment, Δf_1 .

Fig. 13 presents experimental snapshots and the corresponding output data. The snapshots provide a reaction of the robot to each object before and after stepping on it. While the first object was overcome by ZMP control, both the second and third objects were overcome through a combination of stepping control and CAM control in addition to ZMP control. Note that the robot does not step on each object just once, but rather repeatedly steps on them at various positions and angles, leading to continuous exposure to diverse external disturbances.

Based on the data presented in the graph, the balancing process can be explained. During forward walking, the robot repeatedly steps on objects of heights 1.5 cm and 2.0 cm from the start of the 5th DSP at approximately 6.3 s to the end of the 9th DSP at 10.2 s. Throughout this period, the desired ZMP (red line) in the x-direction, z_x^{des} , was generated from approximately 7.1 s to 9 s, up to the ZMP constraint. At around 8 s, a negative x-direction footstep adjustment (blue line), $\Delta f_{x,1}$, of 5.3 cm was generated. Additionally, a small centroidal moment (yellow line), τ_y^{des} , of -0.4 Nm, was created at approximately 7.5 s. In the y-direction, the desired ZMP, z_y^{des} , was generated up to the constraint from approximately 6.9 to 7.8 s, and a small footstep adjustment, $\Delta f_{y,1}$, of 2.4 cm was generated at approximately 7 s.

However, during walking on the 2 cm object after 10.2 s, the robot experienced continuous disturbances such as contact impacts and late landings, leading to instability in its walking. To overcome this disturbance, starting from approximately 10.2 s, the desired ZMP in the y-direction began to be generated up to the ZMP constraint, and the centroidal moment (yellow line), τ_x^{des} , in the x-direction was also generated up to 7 Nm at approximately 10.8 s. Additionally, based on the generated $\Delta f_{y,1}$ of -3 cm at approximately 10.7 s, the stepping controller adjusts the swing foot position (magenta and cyan lines) while optimizing the step time (orange line), T . On the other hand, to control the CP error in the x-direction, CP-MPC primarily generates the desired ZMP, z_x^{des} , with little

utilization of centroidal moment control, τ_y^{des} , or footstep position control, $\Delta f_{x,1}$.

After successfully overcoming these disturbances, at approximately 12.0 s, which is the start of the 11th DSP, the robot steps on the thickest object of 2.5 cm, causing a significant disturbance to the robot. As a result, at approximately 13.6 s, the CP-MPC generates a maximum centroidal moment of -7 Nm and approximately 7.3 cm of $\Delta f_{y,1}$ to overcome the disturbance. Simultaneously, the stepping controller adjusts the robot's swing foot position to the left based on the generated $\Delta f_{y,1}$, while also modifying the step time, T , to approximately 0.8 s in response to significant disturbances. Eventually, the robot maintains its balance. Similar to the results in Section VI-C, disturbances to the robot were relatively larger in the y-direction than in the x-direction. While the robot mainly overcame the disturbances in the x-direction using ZMP control with long support foot length, in the y-direction, both stepping and CAM control were actively used. When using the QP-based method [39], however, the robot could not withstand the disturbance from a 2.5 cm object and fell over.

VII. CONCLUSION

This paper presents a novel balance control framework for humanoid robots to achieve robust balancing performance in the presence of disturbances. The proposed framework utilizes a linear MPC framework to drive three balance strategies, namely ankle, hip, and stepping strategies, for CP tracking control (referred to as CP-MPC). While several humanoid balancing algorithms have been developed to implement the three balance strategies, to the best of our knowledge, this framework is the first MPC-based framework that realizes the three strategies specifically for CP tracking control. The proposed framework effectively calculates ZMP, CAM, and footstep positions to achieve CP tracking control in the presence of disturbances.

In addition, a novel variable weighting method that adjusts the MPC weighting parameters over the time horizon was proposed and applied to the CAM damping control. This method reduced the influence of damping action on CAM control and demonstrated better balancing performance against disturbances compared to the conventional constant weighting method.

Next, a hierarchical structure of CP-MPC and a stepping controller is proposed, enabling step time optimization based on CP-MPC variables. Specifically, the stepping controller adjusts the step time while closely following the footstep adjustments planned by CP-MPC to control the CP offset. The suitability of the parameter selection method used in the stepping controller is validated in comparison to the methods proposed in previous studies [26], [30], [31].

Finally, the balancing performance of the proposed method has been validated through simulations and real robot experiments under various scenarios with disturbances. The robot can traverse uneven terrain and overcome external forces. Notably, the same control parameters were used for both simulations and experiments, resulting in minimal effort for sim-to-real implementation. Furthermore, the superior balancing

performance of the proposed method was experimentally verified, compared with state-of-the-art QP-based CP controller that utilize ankle, hip, and stepping strategies [39].

REFERENCES

- [1] L. M. Nashner and G. McCollum, "The organization of human postural movements: a formal basis and experimental synthesis," *Behavioral and brain sciences*, vol. 8, no. 1, pp. 135–150, 1985.
- [2] D. A. Winter, "Human balance and posture control during standing and walking," *Gait & posture*, vol. 3, no. 4, pp. 193–214, 1995.
- [3] B. E. Maki and W. E. McLroy, "The role of limb movements in maintaining upright stance: the "change-in-support" strategy," *Physical therapy*, vol. 77, no. 5, pp. 488–507, 1997.
- [4] K. Barin, "Evaluation of a generalized model of human postural dynamics and control in the sagittal plane," *Biological cybernetics*, vol. 61, no. 1, pp. 37–50, 1989.
- [5] A. D. Kuo and F. E. Zajac, "Human standing posture: multi-joint movement strategies based on biomechanical constraints," *Progress in brain research*, vol. 97, pp. 349–358, 1993.
- [6] S. Park, F. B. Horak, and A. D. Kuo, "Postural feedback responses scale with biomechanical constraints in human standing," *Experimental brain research*, vol. 154, no. 4, pp. 417–427, 2004.
- [7] S. Kajita, F. Kanehiro, K. Kaneko, K. Yokoi, and H. Hirukawa, "The 3d linear inverted pendulum mode: A simple modeling for a biped walking pattern generation," in *Proceedings 2001 IEEE/RSJ International Conference on Intelligent Robots and Systems. Expanding the Societal Role of Robotics in the Next Millennium (Cat. No. 01CH37180)*, vol. 1. IEEE, 2001, pp. 239–246.
- [8] S. Kajita, F. Kanehiro, K. Kaneko, K. Fujiwara, K. Yokoi, and H. Hirukawa, "Biped walking pattern generation by a simple three-dimensional inverted pendulum model," *Advanced Robotics*, vol. 17, no. 2, pp. 131–147, 2003.
- [9] M. Vukobratović and B. Borovac, "Zero-moment point—thirty five years of its life," *International journal of humanoid robotics*, vol. 1, no. 01, pp. 157–173, 2004.
- [10] M. B. Popovic, A. Goswami, and H. Herr, "Ground reference points in legged locomotion: Definitions, biological trajectories and control implications," *The international journal of robotics research*, vol. 24, no. 12, pp. 1013–1032, 2005.
- [11] S. Kajita, F. Kanehiro, K. Kaneko, K. Fujiwara, K. Harada, K. Yokoi, and H. Hirukawa, "Biped walking pattern generation by using preview control of zero-moment point," in *2003 IEEE international conference on robotics and automation (Cat. No. 03CH37422)*, vol. 2. IEEE, 2003, pp. 1620–1626.
- [12] Y. Choi, D. Kim, and B.-J. You, "On the walking control for humanoid robot based on the kinematic resolution of com jacobian with embedded motion," in *Proceedings 2006 IEEE International Conference on Robotics and Automation, 2006. ICRA 2006*. IEEE, 2006, pp. 2655–2660.
- [13] J.-Y. Kim, I.-W. Park, and J.-H. Oh, "Experimental realization of dynamic walking of the biped humanoid robot khr-2 using zero moment point feedback and inertial measurement," *Advanced Robotics*, vol. 20, no. 6, pp. 707–736, 2006.
- [14] S. Kajita, M. Morisawa, K. Miura, S. Nakaoka, K. Harada, K. Kaneko, F. Kanehiro, and K. Yokoi, "Biped walking stabilization based on linear inverted pendulum tracking," in *2010 IEEE/RSJ International Conference on Intelligent Robots and Systems*. IEEE, 2010, pp. 4489–4496.
- [15] H.-M. Joe and J.-H. Oh, "A robust balance-control framework for the terrain-blind bipedal walking of a humanoid robot on unknown and uneven terrain," *Sensors*, vol. 19, no. 19, p. 4194, 2019.
- [16] T. Komura, H. Leung, S. Kudoh, and J. Kuffner, "A feedback controller for biped humanoids that can counteract large perturbations during gait," in *Proceedings of the 2005 IEEE International Conference on Robotics and Automation*. IEEE, 2005, pp. 1989–1995.
- [17] T. Komura, A. Nagano, H. Leung, and Y. Shinagawa, "Simulating pathological gait using the enhanced linear inverted pendulum model," *IEEE Transactions on biomedical engineering*, vol. 52, no. 9, pp. 1502–1513, 2005.
- [18] J. Pratt, J. Carff, S. Drakunov, and A. Goswami, "Capture point: A step toward humanoid push recovery," in *2006 6th IEEE-RAS international conference on humanoid robots*. IEEE, 2006, pp. 200–207.
- [19] B. Stephens, "Humanoid push recovery," in *2007 7th IEEE-RAS International Conference on Humanoid Robots*. IEEE, 2007, pp. 589–595.
- [20] S.-J. Yi, B.-T. Zhang, D. Hong, and D. D. Lee, "Whole-body balancing walk controller for position controlled humanoid robots," *International Journal of Humanoid Robotics*, vol. 13, no. 01, p. 1650011, 2016.
- [21] G. Wiedebach, S. Bertrand, T. Wu, L. Fiorio, S. McCrory, R. Griffin, F. Nori, and J. Pratt, "Walking on partial footholds including line contacts with the humanoid robot atlas," in *2016 IEEE-RAS 16th International Conference on Humanoid Robots (Humanoids)*. IEEE, 2016, pp. 1312–1319.
- [22] R. Schuller, G. Mesesan, J. Engelsberger, J. Lee, and C. Ott, "Online centroidal angular momentum reference generation and motion optimization for humanoid push recovery," *IEEE Robotics and Automation Letters*, vol. 6, no. 3, pp. 5689–5696, 2021.
- [23] M.-J. Kim, D. Lim, G. Park, and J. Park, "Humanoid balance control using centroidal angular momentum based on hierarchical quadratic programming," in *2022 IEEE/RSJ International Conference on Intelligent Robots and Systems (IROS)*. IEEE, 2022, pp. 6753–6760.
- [24] Y. Ding, C. Khazoom, M. Chignoli, and S. Kim, "Dynamic walking with footstep adaptation on the mit humanoid via linear model predictive control," *arXiv preprint arXiv:2205.15443*, 2022.
- [25] A. Herdt, H. Diedam, P.-B. Wieber, D. Dimitrov, K. Mombaur, and M. Diehl, "Online walking motion generation with automatic footstep placement," *Advanced Robotics*, vol. 24, no. 5-6, pp. 719–737, 2010.
- [26] M. Khadiv, A. Herzog, S. A. A. Moosavian, and L. Righetti, "Step timing adjustment: A step toward generating robust gaits," in *2016 IEEE-RAS 16th International Conference on Humanoid Robots (Humanoids)*. IEEE, 2016, pp. 35–42.
- [27] H. Jeong, O. Sim, H. Bae, K. Lee, J. Oh, and J.-H. Oh, "Biped walking stabilization based on foot placement control using capture point feedback," in *2017 IEEE/RSJ International Conference on Intelligent Robots and Systems (IROS)*. IEEE, 2017, pp. 5263–5269.
- [28] H.-M. Joe and J.-H. Oh, "Balance recovery through model predictive control based on capture point dynamics for biped walking robot," *Robotics and Autonomous Systems*, vol. 105, pp. 1–10, 2018.
- [29] H. Jeong, I. Lee, O. Sim, K. Lee, and J.-H. Oh, "A robust walking controller optimizing step position and step time that exploit advantages of footed robot," *Robotics and Autonomous Systems*, vol. 113, pp. 10–22, 2019.
- [30] M. Khadiv, A. Herzog, S. A. A. Moosavian, and L. Righetti, "Walking control based on step timing adaptation," *IEEE Transactions on Robotics*, vol. 36, no. 3, pp. 629–643, 2020.
- [31] M.-J. Kim, D. Lim, G. Park, and J. Park, "Foot stepping algorithm of humanoids with double support time adjustment based on capture point control," in *2023 IEEE International Conference on Robotics and Automation (ICRA)*. IEEE, 2023, pp. 12 198–12 204.
- [32] P.-B. Wieber, "Trajectory free linear model predictive control for stable walking in the presence of strong perturbations," in *2006 6th IEEE-RAS International Conference on Humanoid Robots*. IEEE, 2006, pp. 137–142.
- [33] M. Shafiee-Ashtiani, A. Yousefi-Koma, and M. Shariat-Panahi, "Robust bipedal locomotion control based on model predictive control and divergent component of motion," in *2017 IEEE International Conference on Robotics and Automation (ICRA)*. IEEE, 2017, pp. 3505–3510.
- [34] J. Ding, S. Xin, T. L. Lam, and S. Vijayakumar, "Versatile locomotion by integrating ankle, hip, stepping, and height variation strategies," in *2021 IEEE International Conference on Robotics and Automation (ICRA)*. IEEE, 2021, pp. 2957–2963.
- [35] J. Ding, L. Han, L. Ge, Y. Liu, and J. Pang, "Robust locomotion exploiting multiple balance strategies: An observer-based cascaded model predictive control approach," *IEEE/ASME Transactions on Mechatronics*, vol. 27, no. 4, pp. 2089–2097, 2022.
- [36] G. Romualdi, S. Dafarra, G. L'Erario, I. Sorrentino, S. Traversaro, and D. Pucci, "Online non-linear centroidal mpc for humanoid robot locomotion with step adjustment," in *2022 International Conference on Robotics and Automation (ICRA)*. IEEE, 2022, pp. 10 412–10 419.
- [37] Z. Aftab, T. Robert, and P.-B. Wieber, "Ankle, hip and stepping strategies for humanoid balance recovery with a single model predictive control scheme," in *2012 12th IEEE-RAS International Conference on Humanoid Robots (Humanoids 2012)*. IEEE, 2012, pp. 159–164.
- [38] F. Nazemi, A. Yousefi-Koma, M. Khadiv, et al., "A reactive and efficient walking pattern generator for robust bipedal locomotion," in *2017 5th RSI International Conference on Robotics and Mechatronics (ICRoM)*. IEEE, 2017, pp. 364–369.
- [39] H. Jeong, I. Lee, J. Oh, K. K. Lee, and J.-H. Oh, "A robust walking controller based on online optimization of ankle, hip, and stepping strategies," *IEEE Transactions on Robotics*, vol. 35, no. 6, pp. 1367–1386, 2019.

- [40] J. Engelsberger, C. Ott, M. A. Roa, A. Albu-Schäffer, and G. Hirzinger, "Bipedal walking control based on capture point dynamics," in *2011 IEEE/RSJ International Conference on Intelligent Robots and Systems*. IEEE, 2011, pp. 4420–4427.
- [41] A. L. Hof, "The 'extrapolated center of mass' concept suggests a simple control of balance in walking," *Human movement science*, vol. 27, no. 1, pp. 112–125, 2008.
- [42] J. Engelsberger, "Combining reduced dynamics models and whole-body control for agile humanoid locomotion," Ph.D. dissertation, Technische Universität München, 2016.
- [43] M. Morisawa, S. Kajita, F. Kanehiro, K. Kaneko, K. Miura, and K. Yokoi, "Balance control based on capture point error compensation for biped walking on uneven terrain," in *2012 12th IEEE-RAS International Conference on Humanoid Robots (Humanoids 2012)*. IEEE, 2012, pp. 734–740.
- [44] R. J. Griffin, G. Wiedebach, S. Bertrand, A. Leonessa, and J. Pratt, "Walking stabilization using step timing and location adjustment on the humanoid robot, atlas," in *2017 IEEE/RSJ International Conference on Intelligent Robots and Systems (IROS)*. IEEE, 2017, pp. 667–673.
- [45] M. Krause, J. Engelsberger, P.-B. Wieber, and C. Ott, "Stabilization of the capture point dynamics for bipedal walking based on model predictive control," *IFAC Proceedings Volumes*, vol. 45, no. 22, pp. 165–171, 2012.
- [46] Y. Kanamiya, S. Ota, and D. Sato, "Ankle and hip balance control strategies with transitions," in *2010 IEEE International Conference on Robotics and Automation*. IEEE, 2010, pp. 3446–3451.
- [47] C. Khazoom and S. Kim, "Humanoid arm motion planning for improved disturbance recovery using model hierarchy predictive control," in *2022 International Conference on Robotics and Automation (ICRA)*. IEEE, 2022, pp. 6607–6613.
- [48] B. Park, M.-J. Kim, E. Sung, J. Kim, and J. Park, "Whole-body walking pattern using pelvis-rotation for long stride and arm swing for yaw angular momentum compensation," in *2020 IEEE-RAS 20th International Conference on Humanoid Robots (Humanoids)*. IEEE, 2021, pp. 47–52.
- [49] P. Kryczka, P. Kormushev, N. G. Tsagarakis, and D. G. Caldwell, "Online regeneration of bipedal walking gait pattern optimizing footstep placement and timing," in *2015 IEEE/RSJ International Conference on Intelligent Robots and Systems (IROS)*. IEEE, 2015, pp. 3352–3357.
- [50] E. Todorov, T. Erez, and Y. Tassa, "Mujoco: A physics engine for model-based control," in *2012 IEEE/RSJ international conference on intelligent robots and systems*. IEEE, 2012, pp. 5026–5033.